Potent Neutralizing Monoclonal Antibodies Directed to Multiple Epitopes on the SARS-CoV-2 Spike

Lihong Liu[1*], Pengfei Wang[1*], Manoj S. Nair[1*], Jian Yu[1*], Yaoxing Huang[1*], Micah A. Rapp[2*], Qian Wang[3*], Yang Luo[1], Vincent Sahi[1], Amir Figueroa[4], Xinzheng V. Guo[5], Gabriele Cerutti[2], Jude Bimela[2], Jason Gorman[6], Tongqing Zhou[6], Peter D. Kwong[6,7], Joseph G. Sodroski[3], Michael T. Yin[8], Zizhang Sheng[1,2], Lawrence Shapiro[1,2,7#], and David D. Ho[1#]

[1]Aaron Diamond AIDS Research Center, Columbia University Vagelos College of Physicians and Surgeons, New York, NY 10032, USA.

[2]Zuckerman Mind Brain Behavior Institute, Columbia University, New York, NY 10027, USA.

[3]Dana-Farber Cancer Institute, Harvard Medical School, Boston, MA 02215, USA.

[4]Department of Microbiology & Immunology Flow Cytometry Core, Columbia University Vagelos College of Physicians and Surgeons, New York, NY 10032, USA.

[5]Human Immune Monitoring Core, Columbia University Vagelos College of Physicians and Surgeons, New York, NY 10032, USA.

[6]Vaccine Research Center, National Institutes of Health, Bethesda, MD 20892, USA.

[7]Department of Biochemistry, Columbia University, New York, NY 10032, USA.

[8]Division of Infectious Diseases, Department of Internal Medicine, Columbia University Vagelos College of Physicians and Surgeons, New York, NY 10032, USA.

[*]Equal contribution. [#]Co-senior authors.

Address correspondence to David D. Ho: dh2994@cumc.columbia.edu

Abstract

The SARS-CoV-2 pandemic rages on with devasting consequences on human lives and the global economy. The discovery and development of virus-neutralizing monoclonal antibodies could be one approach to treat or prevent infection by this novel coronavirus. Here we report the isolation of 61 SARS-CoV-2-neutralizing monoclonal antibodies from 5 infected patients hospitalized with severe disease. Among these are 19 antibodies that potently neutralized the authentic SARS-CoV-2 *in vitro,* 9 of which exhibited exquisite potency, with 50% virus-inhibitory concentrations of 1 to 9 ng/mL. Epitope mapping showed this collection of 19 antibodies to be about equally divided between those directed to the receptor-binding domain (RBD) and those to the N-terminal domain (NTD), indicating that both of these regions at the top of the viral spike are quite immunogenic. In addition, two other powerful neutralizing antibodies recognized quaternary epitopes that are overlapping with the domains at the top of the spike. Cyro-electron microscopy structures of one antibody targeting RBD, a second targeting NTD, and a third bridging RBD and NTD revealed recognition of the closed, "all RBD-down" conformation of the spike. Several of these monoclonal antibodies are promising candidates for clinical development as potential therapeutic and/or prophylactic agents against SARS-CoV-2.

Background

A novel coronavirus, now termed SARS-CoV-2[1,2], has caused nearly 8 million confirmed infections globally, leading to about 450,000 deaths. This pandemic has also put much of the world on pause, with unprecedented disruption of lives and unparalleled damage to the economy. A return to some semblance of normalcy will depend on science to deliver an effective solution,

and the scientific community has responded admirably. Drug development is well underway, and vaccine candidates are entering clinical trials. Another promising approach is the isolation of SARS-CoV-2-neutralizing monoclonal antibodies (mAbs) that could be used as therapeutic or prophylactic agents. The primary target for such antibodies is the viral spike, a trimeric protein[3,4] that is responsible for binding to the ACE2 receptor on the host cell[1,3,5,6]. The spike protein is comprised of two subunits. The S1 subunit has two major structural elements: RBD and NTD; the S2 subunit mediates virus-cell membrane fusion after the RBD engages ACE2. Reports of discovery of neutralizing mAbs that target the RBD have been published recently[7-11]. We now describe our efforts in isolating and characterizing a collection of mAbs that not only target multiple epitopes on the viral spike but also show exquisite potency in neutralizing SARS-CoV-2.

Patient Selection

Forty patients with PCR-confirmed SARS-CoV-2 infection were enrolled in an observational cohort study on virus-neutralizing antibodies. Plasma samples from all subjects were first tested for neutralizing activity against SARS-CoV-2 pseudovirus (Wuhan-Hu-1 spike pseudotyped with vesicular stomatitis virus). Widely varying neutralizing titers were observed, with IC_{50} ranging from a reciprocal plasma dilution of <100 to ~13,000 (Fig. 1a). Five patients were chosen for mAb isolation because their plasma virus-neutralizing titers were among the highest. The clinical characteristics of these 5 cases are summarized in Extended Data Table 1. In brief, all were severely ill with acute respiratory distress syndrome requiring mechanical ventilation. Their ages ranged from 50 to 71. Two were Hispanic females, two were white males, and one was a black male. One patient died, while the others recovered. Importantly, blood for isolation of SARS-CoV-2 mAbs was obtained on day 18 to 32 post onset of symptoms.

Monoclonal Antibody Isolation and Construction

Peripheral blood mononuclear cells from each patient were put through an experimental schema (Extended Data Fig. 1a) starting with cell sorting by flow cytometry. The sorting strategy focused on live memory B lymphocytes that were CD3-negative, CD19-positive, and CD27-positive (Extended Data Fig. 1b). The final step focused on those cells that bound the SARS-CoV-2 spike trimer (S trimer)[4]. S trimer-positive memory B cells were enriched (0.4% to 1.4%) in the 5 patients as compared to a normal health donor (0.2%) (Extended Data Fig. 1c). A total of 602, 325, 14, 147, and 145 such B cells from Patient 1, Patient 2, Patient 3, Patient 4, and Patient 5, respectively, were labelled with a unique hashtag. The cells were then placed into the 10X Chromium (10X Genomics) for single-cell 5'mRNA and V(D)J sequencing to obtain paired heavy (H) and light (L) chain sequences. A careful bioinformatic analysis was carried out on 1,145 paired sequences to downselect "high-confidence" antigen-specific mAbs. A total of 331 mAb sequences were recovered, representing 252 individual clones. Only 6 mAbs were from Patient 3, whereas 44 to 100 mAbs were identified from each of the other patients (Extended Data Table 2). The VH and VL sequences of 252 antibodies (one per clone) were codon-optimized and synthesized, and each VH and VL gene was then cloned into an expression plasmid with corresponding constant region of H chain and L chain of human IgG1, and mAbs were expressed by co-transfection of paired full-length H chain and L chain genes into Expi293 cells. The supernatant from each transfection was collected for the screening assays and antibody purification.

Monoclonal Antibody Screening

All 252 transfection supernatants were screened for binding to S trimer and RBD by enzyme-linked immunosorbent assays (ELISAs), as well as for neutralization against SARS-CoV-2 pseudovirus and live virus. These results are graphically represented in Fig. 1b and tabulated in Extended Data Table 2. It was evident that a substantial percentage of the mAbs in the supernatants bound S trimer, and a subset of those bound RBD. Specifically, 121 supernatants were scored as positive for S trimer binding, yielding an overall hit rate of 48%. Of these, 38 were positive for RBD binding while the remaining 83 were negative. It is interesting to note that none of the 13 trimer-specific mAbs from Patient 5 recognized RBD. In the pseudovirus neutralization screen, 61 supernatants were scored as positive, indicating that half of the trimer-specific mAbs were virus neutralizing. In particular, 15 supernatants retained neutralizing activity even when diluted by 1,000-fold or more. In the screen for neutralization against SARS-CoV-2 (strain USA-WA1/2020), 41 supernatants were scored as positive, including 10 that neutralized the virus completely (+++). Overall, this screening strategy was quite effective in picking up neutralizing mAbs (vertical lines and labelled antibodies at the bottom of Fig. 1b) that were later identified as potent.

Sequence Analysis of S Trimer-Specific Monoclonal Antibodies

Of the 121 mAbs that bound S trimer, 88% were IgG isotype, with IgG1 being predominant (Extended Data Fig. 2a). Small numbers of antibodies of IgM and IgA isotypes were also found. Comparison to the IgG repertoire of three healthy human donors[12], a statistically significant over-representation of IGHV3-30, IGKV3-20, and IGHJ6 genes was observed for this collection of SARS-CoV-2 mAbs (Extended Data Figs. 2b and 2c). A longer CDRH3 length was also noted (Extended Data Fig. 2d). Interestingly, the average percentages of somatic hypermutation in VH

and VL were 2.1 and 2.5, respectively, which were significantly lower than those found in healthy individuals (Extended Data Fig. 2e) and remarkably close to germline sequences.

Antigen Binding and Virus Neutralization

Since the screening for pseudovirus neutralization was performed quantitatively with serial dilutions of the transfection supernatants, we plotted in Extended Data Fig. 3 the best-fit neutralization curves for 130 samples that were positive in at least one of the screens shown in Fig. 1b. Most were non-neutralizing or weakly neutralizing, but 18 showed evidently better potency. One additional supernatant was initially missed in the pseudovirus screen (Patient 1 in Extended Data Fig. 3) but was later found to be a potent neutralizing mAb. Together, these 19 mAbs were purified from transfection supernatants and further characterized for their binding and neutralization properties. As shown in Fig. 2a, all but one (2-43) of the mAbs bound the S trimer by a quantitative ELISA. Using two other quantitative ELISAs, nine of the antibodies clearly bound RBD, with little or no binding to NTD. Eight antibodies bound NTD to varying degrees, with no binding to RBD. Two mAbs bound neither RBD nor NTD, and were therefore categorized as “Others”.

The pseudovirus neutralization profiles for these purified 19 mAbs are shown in the top portion of Fig. 2b. The RBD-directed antibodies neutralized the pseudovirus with IC_{50} of 0.005 to 0.512 μg/mL; the NTD-directed antibodies were slightly less potent, with IC_{50} ranging from 0.013 to 0.767 μg/mL. A common feature of the NTD mAbs was the plateauing of virus neutralization at levels short of 100%. Two antibodies, categorized as “Others”, neutralized with IC_{50} of 0.071 and 0.652 μg/mL, with mAb 2-51 exhibiting the plateauing effect typical of NTD antibodies. Antibody

neutralization of the authentic or live SARS-CoV-2 (strain USA-WA1/2020) was carried out using Vero cells inoculated with a multiplicity of infection of 0.1. As shown in the bottom portion of Fig. 2b, the RBD-directed antibodies again neutralized the virus but with IC_{50} of 0.0007 to 0.209 μg/mL; the NTD-directed antibodies showed similar potency, with IC_{50} ranging from 0.007 to 0.109 μg/mL. Here, the plateauing effect seen in the pseudovirus neutralization assay was less apparent. Antibodies 2-43 and 2-51 neutralized the live virus with IC_{50} of 0.003 and 0.007 μg/mL, respectively. Overall, nine mAbs exhibited exquisite potency in neutralizing authentic SARS-CoV-2 *in vitro* with IC_{50} of 0.009 μg/mL or less, including four directed to RBD (2-15, 2-7, 1-57, and 1-20), three to NTD (2-17, 5-24, and 4-8), and two to undetermined regions on the S trimer (2-43 and 2-51). It is remarkable that Patient 2 alone contributed five of the top nine SARS-CoV-2 neutralizing mAbs.

Epitope Mapping

All 19 potent neutralizing mAbs (Fig. 2) were further studied in antibody competition experiments to gain insight into their epitopes. In addition, 12 mAbs that bound the S trimer strongly during the initial supernatant screen were also chosen, including 5 that bound RBD (1-97, 2-26, 4-13, 4-24, and 4-29) and 7 that did not bind RBD (1-21, 2-29, 4-15, 4-32, 4-33, 4-41, and 5-45). Four of these mAbs were weak in neutralizing SARS-CoV-2 pseudovirus, and the remaining 8 were non-neutralizing (Extended Data Fig. 4). First, a total of 16 non-RBD mAbs were evaluated for competition in binding to S trimer by ELISA in a "checkerboard" experiment. The extent of the antibody competition is reflected by the intensity of the heatmap shown in Fig. 3a, left panel. There is one large cluster (A) of mAbs that competed with one another, and it partially overlaps a small cluster (B). A third cluster (C) does not overlap at all. Note that all but one of the antibodies

in cluster A recognized NTD. Antibody 2-51 is clearly directed to the NTD region even though it could not bind NTD. Moreover, one mAb each from clusters B and C also recognized NTD, thereby indicating that all three clusters are within or near the NTD. One mAb, 1-21, appears to have a unique non-overlapping epitope (epitope region D).

Second, a similar "checkerboard" competition experiment was carried out by ELISA for 14 of our RBD-directed mAbs plus CR3022[13,14]. Here, the heatmap shows that there are four epitope clusters that are serially overlapping (Fig. 3a, right panel). There is one large cluster (E) that contains mAbs largely capable of blocking ACE2 binding. Furthermore, 4 antibodies in this cluster lost binding to a mutant RBD (L455R, A475R, G502R) that could no longer bind ACE2 (our unpublished findings). Taken together, these results suggest that most of the mAbs in cluster E are directed to the ACE2-binding interface of RBD. The next cluster (F) connects to both cluster E and cluster G, the location of which is defined by its member CR3022[15]. Lastly, cluster G overlaps another cluster (H), which includes 1-97 that strongly inhibited the binding of 2-30 to the S trimer. This finding suggests that cluster H may be proximal to one edge of cluster E.

One potent neutralizing mAb, 2-43, did not bind S trimer by ELISA (Fig. 2a) and thus could not be tested in the above competition experiments. However, 2-43 did strongly bind S trimer when expressed on the cell surface as determined by flow cytometry, and this binding was competed out by itself but not by RBD, NTD, ACE2, or the soluble S trimer[4] (Extended Data Fig. 5). NTD-directed mAbs had only a modest effect on its binding to cell-surface S trimer, but numerous RBD-directed mAbs in cluster E potently blocked the binding of 2-43, demonstrating that this antibody

is likely targeting a quaternary epitope on the top of RBD that includes a portion of the interface with ACE2.

The results in Fig. 3a and Extended Data Fig. 5 could be represented by two sets of Venn diagrams shown in Fig. 3b. In the non-RBD region, the potent neutralizing mAbs reside exclusively in cluster A and bind a patch on the NTD. Weaker neutralizing mAbs recognize a region at the interface between clusters A and B. In the RBD region, the most potent neutralizing mAbs also group together within one cluster (E). Given that all block ACE2 binding, it is likely they recognize the top of RBD and neutralize the virus by competitive inhibition of receptor binding. Cluster G contains CR3022, a mAb known to be directed to an epitope on a cryptic site on the side of RBD when it is in the "up" position[15]. Cluster F is therefore likely situated between the top and this "cryptic" site. The Venn diagram also suggests that cluster H may occupy a different side surface near the top of RBD, perhaps in the region recognized by S309[8].

Cryo-Electron Microscopy

To further understand antibody recognition of the viral spike and to aid the interpretation of the mapping studies, we determined cryo-EM structures of Fabs from three mAbs in complex with the S trimer[4]. First, single-particle analysis of the complex with 2-4 Fab (RBD-directed) yielded maps of high quality (Fig. 4a; Extended Data Table 3; Extended Data Fig. 6), with the most abundant particle class representing a 3-Fab-per-trimer complex, refined to an overall resolution of 3.2 Å. While density for the constant portion of the Fabs was visible, it was blurred due to molecular motion, and thus only the variable domains were included in the molecular model. Fab of 2-4 bound the spike protein near the apex, with all RBDs in the "down" orientation, and the structure

of the antibody-bound spike protein was highly similar to previously published unliganded spike structures in the "all-down" conformation[3,4]. The 2-4 epitope on RBD has a buried surface area of 751 Å^2, sharing 284 Å^2 with the interface of ACE2. Detailed interactions between 2-4 and RBD, along with comparative analyses, are discussed and exhibited in Extended Data Fig. 7. Overall, Fig. 4a shows that neutralization of SARS-CoV-2 by mAb 2-4 likely results from locking RBD in the down conformation while also occluding access to ACE2.

Second, we also produced 3D cryo-EM reconstructions of the Fab of 4-8 (NTD-directed) in complex with the S trimer (Extended Data Table 3; Extended Data Fig. 8). Two main particle classes were observed – one for a 3-Fab-bound complex with all RBDs "down" at 3.9 Å resolution (Fig. 4b), and another a 3-Fab-bound complex with one RBD "up" at 4.0 Å resolution (Extended Data Fig. 9). However, molecular motion prevented visualization of the interaction at high resolution. Nevertheless, the density in the 4-8 map reveals the overall positions of the antibody chains targeting NTD, and helps to anchor the results of the antibody competition experiments. How such binding to the tip of NTD results in SARS-CoV-2 neutralization remains unclear.

Third, a 7.8 Å resolution reconstructions of the Fab of 2-43 in complex with the S trimer (Extended Data Table 3; Extended Data Fig. 10) revealed three bound Fabs, each targeting a quaternary epitope on the top of the spike that included the RBD of one protomer and the NTD of another (Fig. 4c), consistent with the epitope mapping results (Extended Data Fig. 5 and Fig. 3b). Given these findings, the inability of 2-43 to bind S trimer by ELISA is likely an artifact of the assay format, as this mAb did bind the spike expressed on the cell surface and in the cryo-EM study.

Fig. 4c suggests that 2-43 could block SARS-CoV-2 infection by occluding the site necessary for ACE2 binding.

Armed with these three cryo-EM reconstructions, we used the Venn diagrams from Fig. 3b to map the epitopes of many of our SARS-CoV-2 neutralizing mAbs onto the surface of the spike (Fig. 4d). This is obviously a rough approximation since antibody footprints are much larger than the area occupied by the mAb number. However, the spatial relationship of the antibody epitopes should be reasonably represented by Fig. 4d.

Discussion

We have discovered a collection of SARS-CoV-2-neutralizing mAbs that are not only potent but also diverse. Nine of these antibodies can neutralize the authentic virus *in vitro* at concentrations of 9 ng/mL of less (Fig. 2b), including 4 directed to RBD, 3 directed to NTD, and 2 to quaternary epitopes nearby. Surprisingly, many of the these mAbs have V(D)J sequences close to germline sequences, without extensive somatic hypermutations (Extended Data Fig. 2e), a finding that bodes well for vaccine development. Our most potent RBD-specific mAbs (e.g., 2-15, 2-7, 1-57, and 1-20) compare favorably with such antibodies recently reported[7,8,10,16-20], including those with high potency[9,11,21,22]. It appears from the epitope mapping studies that mAbs directed to the top of RBD strongly compete with ACE2 binding and potently neutralize the virus, whereas those directed to the side surfaces of RBD do not compete with ACE2 and neutralize less potently (Figs. 3b and 4d). Our collection of non-RBD neutralizing mAbs is unprecedented in that such antibodies only have been sporadically reported and only with substantially lower potencies[22-24]. The most potent of these mAbs are directed to (e.g., 2-17, 5-24, and 4-8) or overlapping with (2-51) a patch on the NTD (Figs. 3b and 4d). It is unclear how NTD-directed mAbs block SARS-CoV-2 infection and

why their neutralization profiles are different from those of RBD-directed antibodies (Fig. 2b). Nevertheless, vaccine strategies that do not include NTD will be unable to induce an important class of virus-neutralizing antibodies.

The isolation of two mAbs (2-43 and 2-51) directed to epitopes that do not map to RBD and NTD is also unprecedented. Cryo-EM of 2-43 bound to the S trimer has confirmed its epitope as quaternary in nature, crossing from the top of RBD to the top of an adjacent NTD (Fig. 4c). It will be equally informative to understand the epitope of 2-51 as well. In this study, we also show the first evidence by cryo-EM for a neutralizing mAb (4-8) bound to the NTD of the viral spike (Fig. 4b), as well as another high-resolution structure of a mAb (2-4) bound to RBD (Fig. 4a). Collectively, these findings will contribute to the understanding of how antibodies bind and neutralize SARS-CoV-2.

The potency and diversity of our SARS-CoV-2-neutralizing mAbs are likely attributable to patient selection. Previously, we observed that infected individuals with severe disease developed a more robust virus-neutralizing antibody response[25]. If Patient 2 had not been included, five of the top neutralizing mAbs would be lost. The diversity of our antibodies is also attributable, in part, to the choice of using the S trimer to sort from memory B cells, while most groups focused on the use of RBD[7,9-11,16-19,21]. The characterization of this diverse collection of mAbs has allowed us to observe that all potent SARS-CoV-2-neutralizing antibodies described to date are directed to the top of the viral spike. RBD and NTD are, no doubt, quite immunogenic. Neutralizing antibodies to the stem region of the S trimer remain to be discovered. In conclusion, we believe several of

273 our monoclonal antibodies with exquisite virus-neutralizing activity are promising candidates for

274 development as modalities to treat or prevent SARS-CoV-2 infection.

References

1 Zhou, P. *et al.* A pneumonia outbreak associated with a new coronavirus of probable bat origin. *Nature* **579**, 270-273, doi:10.1038/s41586-020-2012-7 (2020).

2 Wang, C., Horby, P. W., Hayden, F. G. & Gao, G. F. A novel coronavirus outbreak of global health concern. *Lancet* **395**, 470-473, doi:10.1016/S0140-6736(20)30185-9 (2020).

3 Walls, A. C. *et al.* Structure, Function, and Antigenicity of the SARS-CoV-2 Spike Glycoprotein. *Cell* **181**, 281-292 e286, doi:10.1016/j.cell.2020.02.058 (2020).

4 Wrapp, D. *et al.* Cryo-EM structure of the 2019-nCoV spike in the prefusion conformation. *Science* **367**, 1260-1263, doi:10.1126/science.abb2507 (2020).

5 Hoffmann, M. *et al.* SARS-CoV-2 Cell Entry Depends on ACE2 and TMPRSS2 and Is Blocked by a Clinically Proven Protease Inhibitor. *Cell* **181**, 271-280 e278, doi:10.1016/j.cell.2020.02.052 (2020).

6 Wang, Q. *et al.* Structural and Functional Basis of SARS-CoV-2 Entry by Using Human ACE2. *Cell* **181**, 894-904 e899, doi:10.1016/j.cell.2020.03.045 (2020).

7 Ju, B. *et al.* Human neutralizing antibodies elicited by SARS-CoV-2 infection. *Nature*, doi:10.1038/s41586-020-2380-z (2020).

8 Pinto, D. *et al.* Cross-neutralization of SARS-CoV-2 by a human monoclonal SARS-CoV antibody. *Nature*, doi:10.1038/s41586-020-2349-y (2020).

9 Cao, Y. *et al.* Potent neutralizing antibodies against SARS-CoV-2 identified by high-throughput single-cell sequencing of convalescent patients' B cells. *Cell*, doi:10.1016/j.cell.2020.05.025 (2020).

10 Wu, Y. *et al.* A noncompeting pair of human neutralizing antibodies block COVID-19 virus binding to its receptor ACE2. *Science* **368**, 1274-1278, doi:10.1126/science.abc2241 (2020).

11 Hansen, J. *et al.* High-Throughput Effort Using Both Humanized Mice and Convalescent Humans Yields SARS-CoV-2 Antibody Cocktail. *Science*, doi:in press (2020).

12 Sheng, Z. *et al.* Gene-Specific Substitution Profiles Describe the Types and Frequencies of Amino Acid Changes during Antibody Somatic Hypermutation. *Front Immunol* **8**, 537, doi:10.3389/fimmu.2017.00537 (2017).

13 ter Meulen, J. *et al.* Human monoclonal antibody combination against SARS coronavirus: synergy and coverage of escape mutants. *Plos Med* **3**, e237, doi:10.1371/journal.pmed.0030237 (2006).

14 Tian, X. *et al.* Potent binding of 2019 novel coronavirus spike protein by a SARS coronavirus-specific human monoclonal antibody. *Emerg Microbes Infect* **9**, 382-385, doi:10.1080/22221751.2020.1729069 (2020).

15 Yuan, M. *et al.* A highly conserved cryptic epitope in the receptor binding domains of SARS-CoV-2 and SARS-CoV. *Science* **368**, 630-633, doi:10.1126/science.abb7269 (2020).

16 Rogers, T. F. *et al.* Rapid isolation of potent SARS-CoV-2 neutralizing antibodies and protection in a small animal model. *bioRxiv*, doi:10.1101/2020.05.11.088674 (2020).

17 Chen, X. *et al.* Human monoclonal antibodies block the binding of SARS-CoV-2 spike protein to angiotensin converting enzyme 2 receptor. *Cell Mol Immunol* **17**, 647-649, doi:10.1038/s41423-020-0426-7 (2020).

18 Zeng, X. *et al.* Isolation of a human monoclonal antibody specific for the receptor binding domain of SARS-CoV-2 using a competitive phage biopanning strategy. *Antibody Therapeutics* **3**, 95-100, doi:10.1093/abt/tbaa008 (2020).

19 Liu, X. *et al.* Neutralizing Antibodies Isolated by a site-directed Screening have Potent Protection on SARS-CoV-2 Infection. *bioRxiv*, 2020.2005.2003.074914, doi:10.1101/2020.05.03.074914 (2020).

20 Zost, S. J. *et al.* Rapid isolation and profiling of a diverse panel of human monoclonal antibodies targeting the SARS-CoV-2 spike protein. *bioRxiv*, doi:10.1101/2020.05.12.091462 (2020).

21 Robbiani, D. F. *et al.* Convergent Antibody Responses to SARS-CoV-2 Infection in Convalescent Individuals. *bioRxiv*, doi:10.1101/2020.05.13.092619 (2020).

22 Brouwer, P. J. M. *et al.* Potent neutralizing antibodies from COVID-19 patients define multiple targets of vulnerability. *bioRxiv*, 2020.2005.2012.088716, doi:10.1101/2020.05.12.088716 (2020).

23 Chi, X. *et al.* A potent neutralizing human antibody reveals the N-terminal domain of the Spike protein of SARS-CoV-2 as a site of vulnerability. *bioRxiv*, 2020.2005.2008.083964, doi:10.1101/2020.05.08.083964 (2020).

24 Wang, C. *et al.* A human monoclonal antibody blocking SARS-CoV-2 infection. *Nat Commun* **11**, 2251, doi:10.1038/s41467-020-16256-y (2020).

25 Wang, P. *et al.* SARS-CoV-2 Neutralizing Antibody Responses Are More Robust in Patients with Severe Disease. *bioRxiv*, 2020.2006.2013.150250, doi:10.1101/2020.06.13.150250 (2020).

Figures and Legends

Fig. 1a

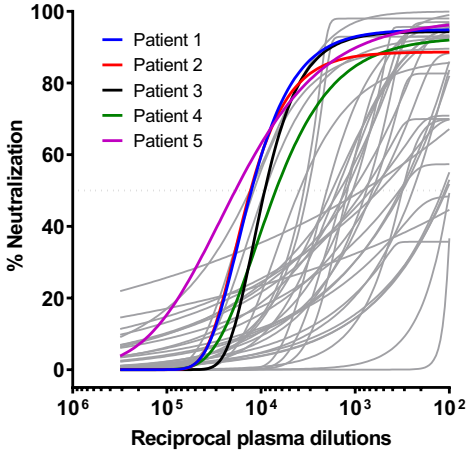

Fig. 1b

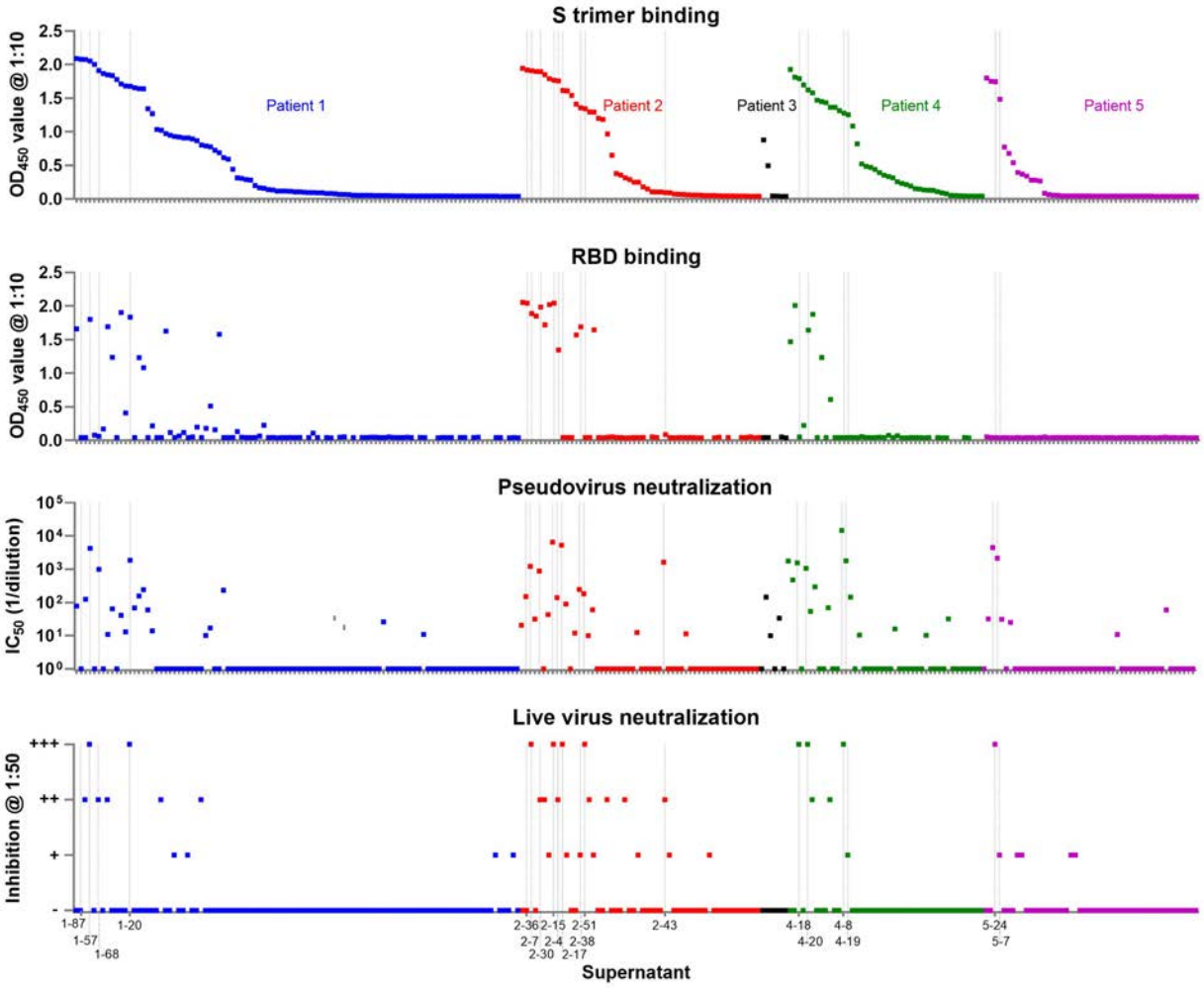

Fig. 1 Isolation of SARS-CoV-2 mAbs from infected patients with severe disease. a, Plasma neutralization profile of 40 patients against SARS-CoV-2 pseudovirus (highlighted are 5 top neutralizers chosen). **b**, All 252 transfection supernatants were screened for binding to S trimer and RBD, as well as for neutralization against SARS-CoV-2 pseudovirus and live virus. For pseudovirus neutralization, the 50% inhibitory dilutions (IC_{50}) of each supernatant were plotted. For live virus, semi-quantitative representation of the inhibition at a dilution of 1:50, with neutralization levels ranging from (-) for none to (+++) for complete neutralization, was plotted. Potent antibodies later identified are marked by vertical lines and labelled at the bottom. The antibodies from each patient are colored as in **a**.

Fig. 2a

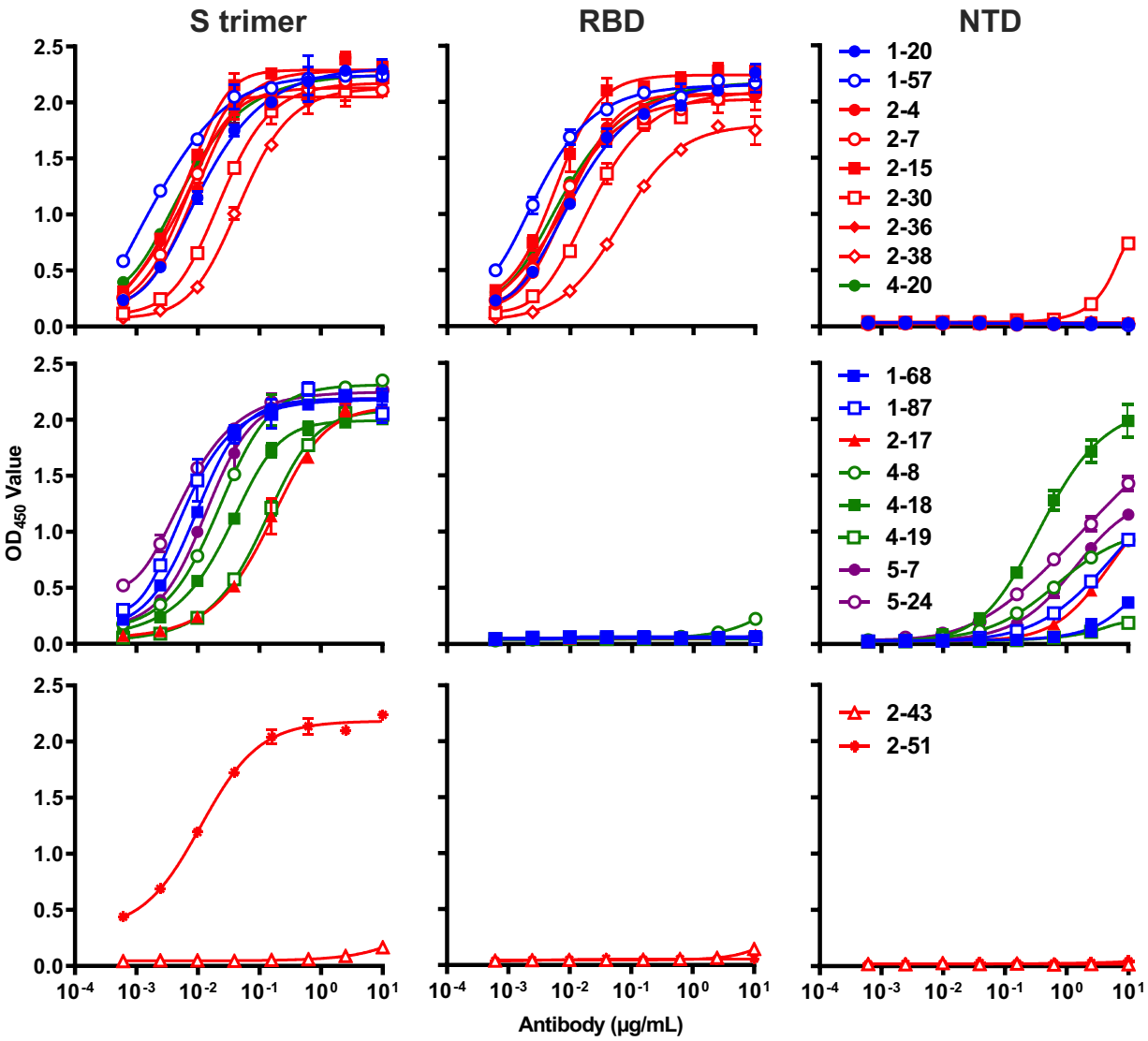

350

Fig. 2b

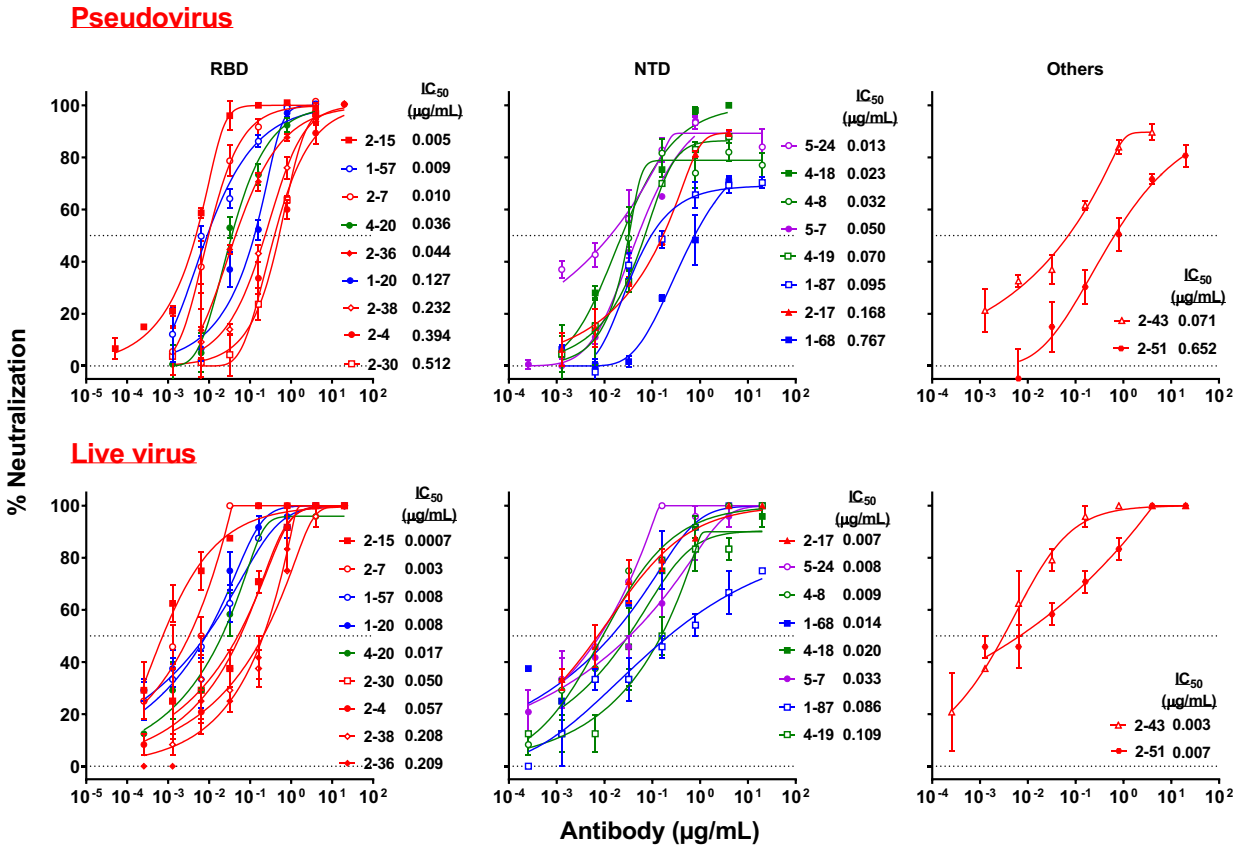

Fig. 2 Characterization of SARS-CoV-2 potent neutralizing mAbs. a, Binding profiles of 19 purified potent neutralizing mAbs against SARS-CoV-2 S trimer (left), RBD (middle), and NTD (right). Note that mAb 2-30 bound multiple proteins at high concentrations. **b**, The pseudovirus (top panels) and live virus (bottom panels) neutralization profiles for the 19 purified mAbs. Epitope classifications are listed on top of the panel b. Single replicate of the binding experiment and triplicates of neutralization are presented as mean ± SEM.

Fig. 3a

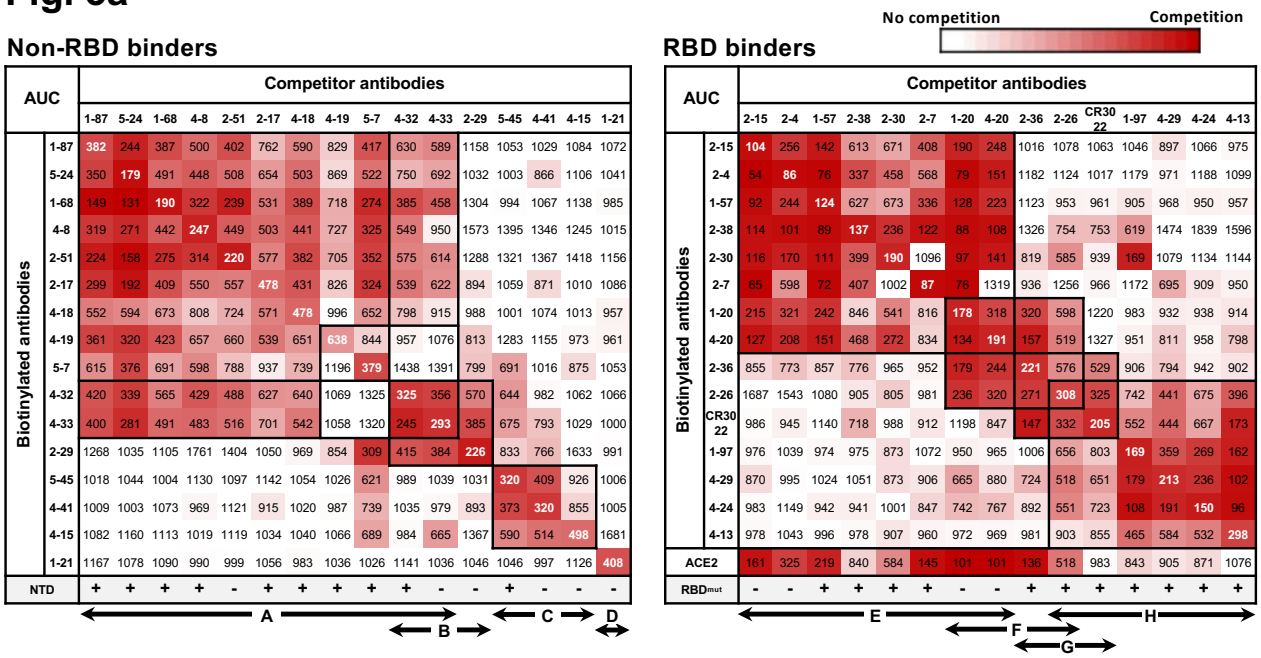

Fig. 3b

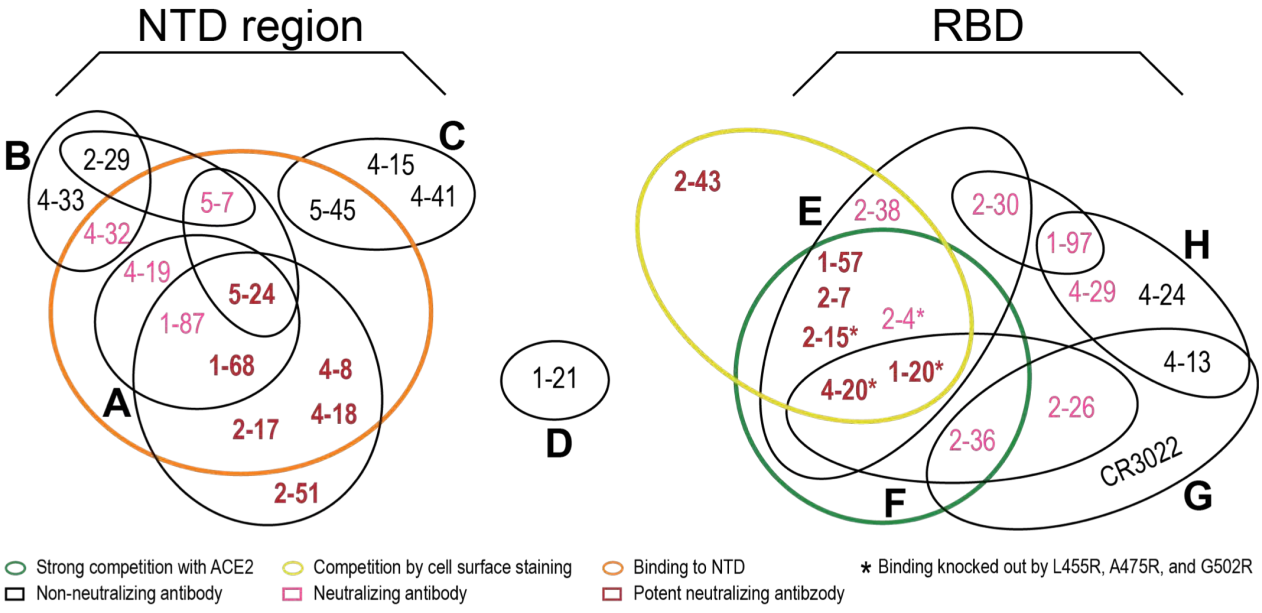

Fig. 3 Epitope mapping of select neutralizing and non-neutralizing mAbs. a, competition results of non-RBD binders (left) and RBD binders (right) in blocking ACE2 or biotinylated mAb binding to the S trimer. In addition, the ability to bind NTD and RBD_{mut} of each mAb is shown. The numbers in each box show the area under each competition curve (AUC) as tested by ELISA. +/- indicates binding/no binding of the mAb to the protein. **b**, Venn diagram interpretation of results from **a** and Extended Data Fig. 5.

Fig. 4a

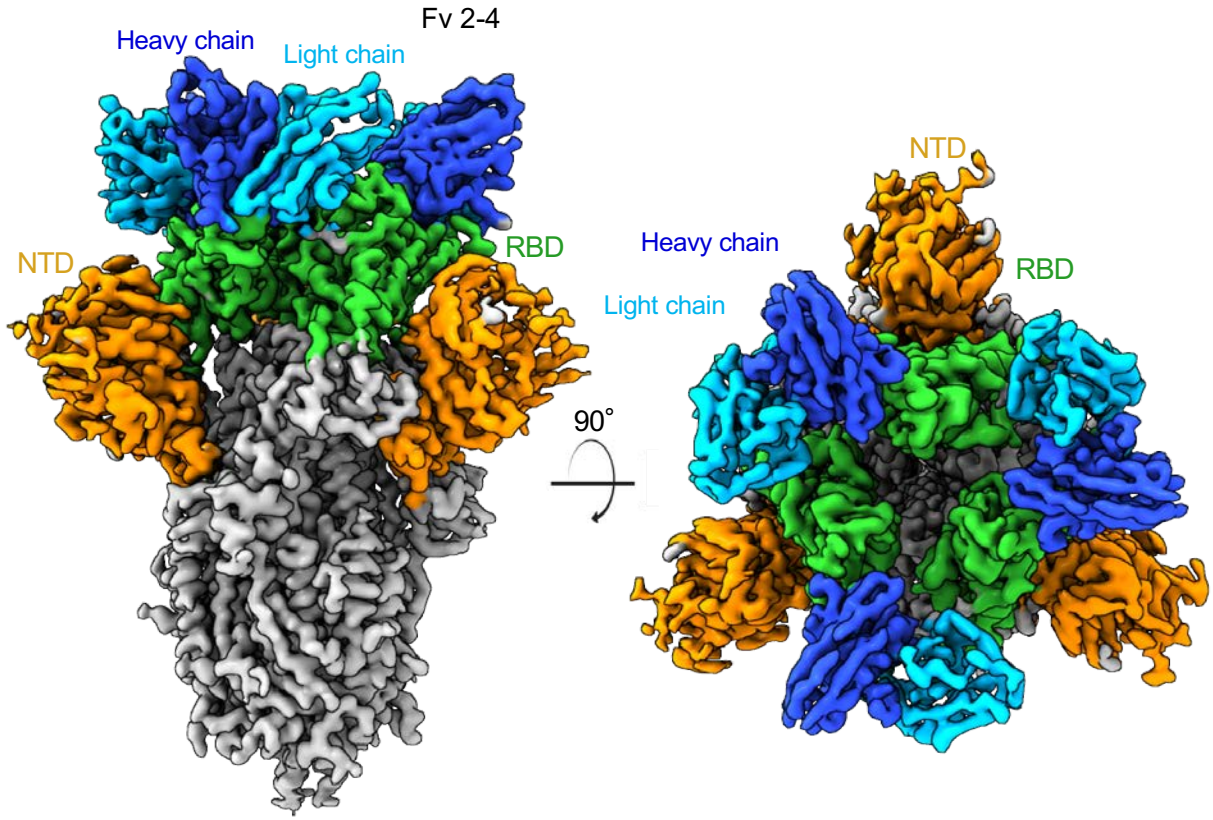

Fig. 4b

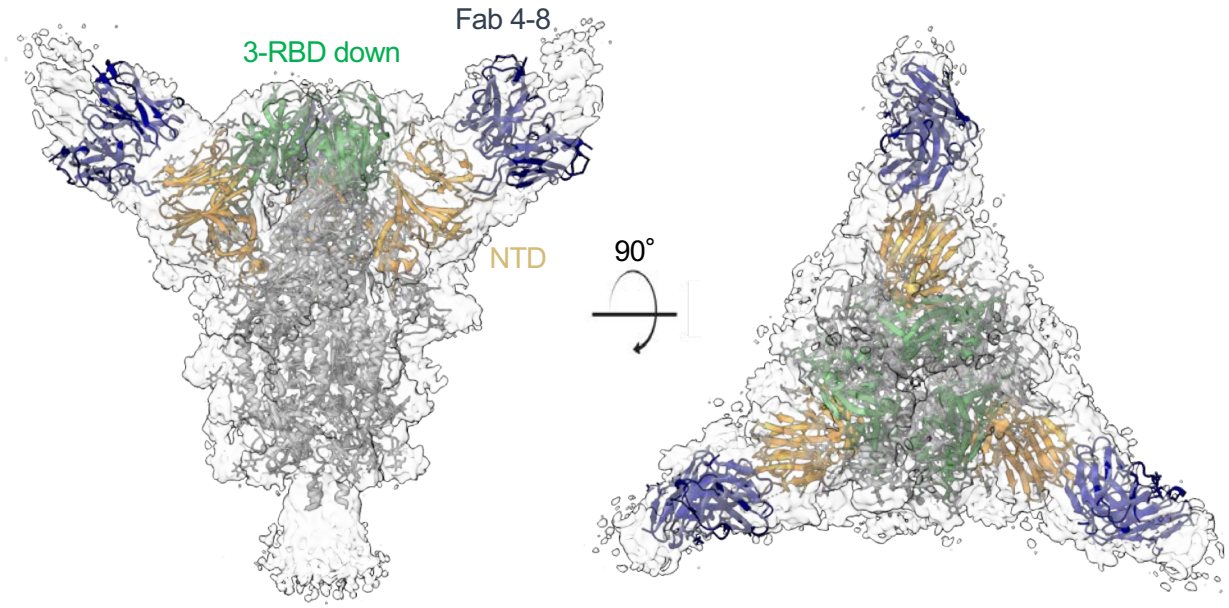

Fig. 4c

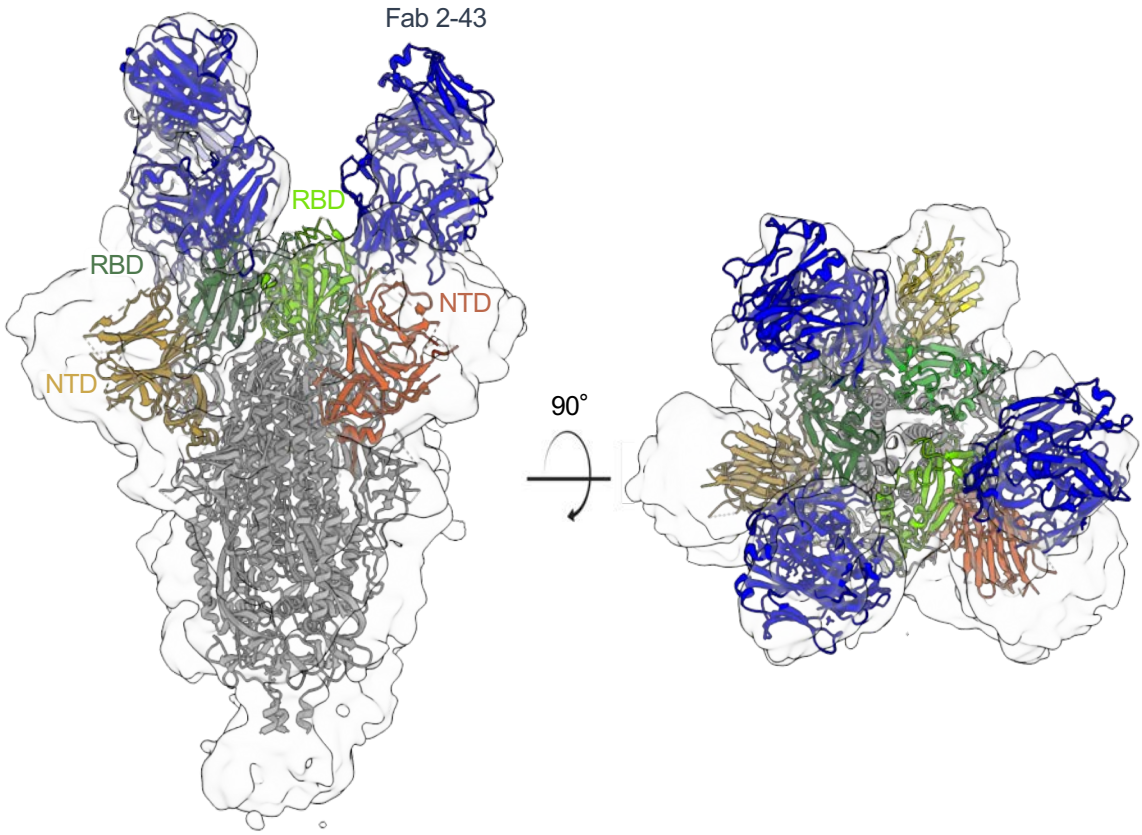

Fig. 4d

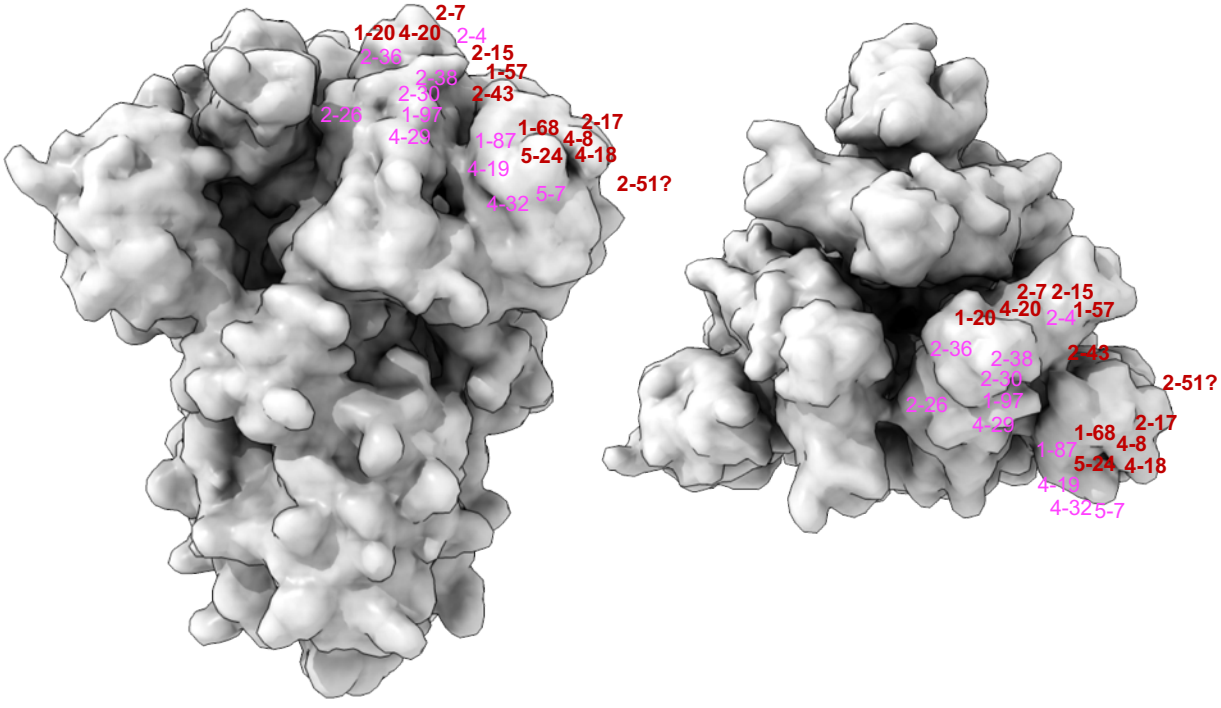

366 **Figure 4. Cryo-EM reconstructions of Fab-spike complexes and visualization of neutralizing**
367 **epitopes on the spike surface. a**, Cryo-EM 3D reconstruction of antibody 2-4 in complex with S
368 trimer at 3.2 Å overall resolution. Density is colored according to spike domain with RBD in green,
369 NTD in orange, with other regions colored grey. **b**, Cryo-EM reconstruction of antibody 4-8 in
370 complex with S trimer (ribbon diagram, colored as in **a**) at 3.9 Å overall resolution, with RBDs in
371 the "all-down" configuration. The resolution of antibody density is limited by molecular motion.
372 Although the binding of Fab to NTD and antibody position are clear, the identities of heavy and
373 light chain are uncertain. **c**, Cryo-EM reconstruction of the antibody 2-43 in complex with S trimer
374 at 7.8 Å resolution reveals a quaternary epitope involving RBD from one subunit and NTD from
375 the next. **d**, Mapping of the Venn diagrams from Fig. 3b onto the surface of the viral spike.

Methods

Expression and Purification of SARS-CoV-2 Proteins

The mammalian expression vector that encodes the ectodomain of the SARS-CoV-2 S trimer and the vector encoding RBD fused with SD1 at the N-terminus and an HRV-3C protease cleavage site followed by a mFc tag and an 8xHis tag at the C-terminus were kindly provided by Jason McLellan[4]. SARS-CoV-2 NTD (aa1-290) with an HRV-3C protease cleavage site, a mFc tag, and an 8xHis tag at the C-terminus was also cloned into mammalian expression vector pCAGGS. Each expression vector was transiently transfected into Expi293 cells using 1 mg/mL of polyethylenimine (Polysciences). Five days post transfection, the S trimer was purified using Strep-Tactin XT Resin (Zymo Research), and the RBD-mFc and NTD-mFc were purified using protein A agarose (ThermoFisher Scientific). In order to obtain RBD-SD1 and NTD, the mFc and 8xHis tags at the C-terminus were removed by HRV-3C protease (Millipore-Sigma) and then purified using Ni-NTA resin (Invitrogen) followed by protein A agarose.

Sorting for S Trimer-Specific B cells and Single-Cell BCR Sequencing

Peripheral blood mononuclear cells from five patients and one healthy donor were stained with LIVE/DEAD™ Fixable Yellow Dead Cell Stain Kit (Invitrogen) at ambient temperature for 20 mins, followed by washing with RPMI-1640 complete medium and incubation with 10 μg/mL of S trimer at 4˚C for 45 mins. Afterwards, the cells were washed again and incubated with a cocktail of flow cytometry and hashtag antibodies, containing CD3 PE-CF594 (BD Biosciences), CD19 PE-Cy7 (Biolegend), CD20 APC-Cy7 (Biolegend), IgM V450 (BD Biosciences), CD27 PerCP-Cy5.5 (BD Biosciences), anti-His PE (Biolegend), and human Hashtag 3 (Biolegend) at 4˚C for 1

hr. Stained cells were then washed, resuspended in RPMI-1640 complete medium and sorted for S trimer-specific memory B cells (CD3-CD19+CD27+S trimer+ live single lymphocytes). The sorted cells were mixed with mononuclear cells from the same donor, labeled with Hashtag 1, and loaded into the 10X Chromium chip of the 5' Single Cell Immune Profiling Assay (10X Genomics) at the Columbia University Human Immune Monitoring Core (HIMC; RRID:SCR_016740). The library preparation and quality control were performed according to manufacturer's protocol and sequenced on a NextSeq 500 sequencer (Illumina).

Identification of S Trimer-Specific Antibody Transcripts

For each sample, full-length antibody transcripts were assembled using the VDJ module in Cell Ranger (version 3.1.0, 10X Genomics) with default parameters and the GRCh38 genome as reference. To identify cells from the antigen sort, we first used the count module in Cell Ranger to calculate copies of all hashtags in each cell from the Illumina NGS raw reads. High confidence antigen-specific cells were identified as follows. Briefly, based on the copy numbers of the hashtags observed, a cell must contain more than 100 copies of the antigen sort-specific hashtag to qualify as an antigen-specific cell. Because hashtags can fall off from cells and bind to cells from a different population in the sample mixture, each cell usually has both sorted and spiked-in-specific hashtags. To enrich for true antigen-specific cells, the copy number of the specific hashtag has to be at least 1.5x higher than that of the non-specific hashtag. Low quality cells were identified and removed using the cell-calling algorithm in Cell Ranger. Cells that do not have productive H and L chain pairs were excluded. If a cell contains more than two H or/and L chain transcripts, the transcripts with less than 3 unique molecular identifiers were removed. Cells with identical H and L chain sequences, which may have resulted from mRNA leakage, were merged

into one cell. Additional filters were applied to remove low quality cells and/or transcripts in the antibody gene annotation process.

Antibody Transcript Annotation and Selection Criteria

Antigen-specific antibody transcripts were processed using our bioinformatics pipeline SONAR for quality control and annotation[26]. Briefly, V(D)J genes were assigned for each transcript using BLAST[27] with customized parameters against a germline gene database obtained from the international ImMunoGeneTics information system (IMGT) database[26,28]. Based on BLAST alignments of V and J regions, CDR3 was identified using the conserved second cysteine in the V region and WGXG (H chain) or FGXG (L chain) motifs in the J region (X represents any amino acid). For H chain transcripts, the constant domain 1 (CH1) sequences were used to assign isotype using BLAST with default parameters against a database of human CH1 genes obtained from IMGT. A BLAST E-value threshold of 1E-6 was used to find significant isotype assignments, and the CH1 allele with the lowest E-value was used. Sequences other than the V(D)J region were removed and transcripts containing incomplete V(D)J or/and frame shift were excluded. We then aligned each of the remaining transcripts to the assigned germline V gene using CLUSTALO[29] and calculated the somatic hypermutation level.

To select representative antibodies for functional characterization, we first clustered all antibodies using USEARCH[30] with the following criteria: identical heavy chain V and J gene assignments, the same length of CDRH3, and CDRH3 identity higher than 0.9. For each cluster, cells with the same light chain V and J gene assignments were grouped into a clone. All clone assignments were manually checked. We then calculated the clonal size for each clone, and one H and L chain pair

per clone was chosen for antibody synthesis. For clones with multiple members, the member with the highest somatic hypermutation level was chosen for synthesis. For cells having multiple high quality H or L chains, which may be from doublets, we synthesized all H and L chain combinations.

Analysis of S Trimer-Specific Antibody Repertoire

Because 88% of the S trimer-specific antibodies were IgG isotype, we therefore compared the repertoire features to IgG repertoires from three healthy donors[31] (17,243 H chains, 27,575 kappa L chains, 20,889 lambda L chains). The repertoire data from the three healthy donors were combined and annotated using SONAR with the same process as above.

Antibody Expression and Purification

For each antibody, variable genes were optimized for human cell expression and synthesized by GenScript. VH and VL were inserted separately into plasmids (gWiz or pcDNA3.4) that encode the constant region for H chain and L chain. Monoclonal antibodies were expressed in Expi293 (ThermoFisher, A14527) by co-transfection of H chain and L chain expressing plasmids using polyethylenimine and culture in 37°C shaker at 125 RPM and 8% CO_2. On day 3 post transfection, 400 µL of supernatant were collected for screening for binding to S trimer and RBD by ELISA, and for neutralization of SARS-CoV-2 pseudovirus and authentic virus. Supernatants were also collected on day 5 for antibody purification by rProtein A Sepharose (GE, 17-1279-01) affinity chromatography.

Production of Pseudoviruses

Recombinant Indiana VSV (rVSV) expressing SARS-CoV-2 spike was generated as previously described[32,33]. HEK293T cells were grown to 80% confluency before transfection with pCMV3-SARS-CoV-2-spike (Sino Biological) using FuGENE 6 (Promega). Cells were cultured overnight at 37°C with 5% CO_2. The next day, medium was removed and VSV-G pseudotyped ΔG-luciferase (G*ΔG-luciferase, Kerafast) was used to infect the cells in DMEM at a MOI of 3 for 1 hr before washing the cells with 1X DPBS three times. DMEM supplemented with 2% fetal bovine serum and 100 I.U./mL of penicillin and 100 µg/mL of streptomycin were added to the inoculated cells, which were cultured overnight as described above. The supernatant was harvested the following day and clarified by centrifugation at 300 g for 10 mins before aliquoting and storing at −80°C.

Pseudovirus Neutralization

Neutralization assays were performed by incubating pseudoviruses with serial dilutions of heat-inactivated plasma together with supernatant or purified antibodies, and scored by the reduction in luciferase gene expression. In brief, Vero E6 cells (ATCC) were seeded in a 96-well plate at a concentration of 2×10^4 cells per well. Pseudoviruses were incubated the next day with serial dilutions of the test samples in duplicate or triplicate for 30 mins at 37°C. The mixture was added to cultured cells and incubated for an additional 24 hrs. The luminescence was measured by Britelite plus Reporter Gene Assay System (PerkinElmer). IC_{50} was defined as the dilution at which the relative light units were reduced by 50% compared with the virus control wells (virus + cells) after subtraction of the background in the control groups with cells only. The IC_{50} values were calculated using non-linear regression in GraphPad Prism 8.0.

Authentic SARS-CoV-2 Neutralization

Supernatants containing expressed mAbs were diluted 1:10 and 1:50 in EMEM with 7.5% inactivated fetal calf serum and incubated with authentic SARS-CoV-2 (strain USA-WA1/2020; MOI 0.1) for 1hr at 37°C. Post-incubation, the mixture was transferred onto a monolayer of Vero-E6 cells that was cultured overnight. After incubation of the cells with the mixture for 70 hrs at 37°C, cytopathic effects (CPE) caused by the infection were scored for each well from 0 to 4 to indicate the degree of virus inhibition. Semi-quantitative representation of the inhibition for each antibody-containing supernatant at a dilution of 1:50 is shown in the lowest panel of Fig. 1b with neutralization levels ranging from (-) for none to (+++) for complete neutralization.

An end-point dilution assay in a 96-well plate format was performed to measure the neutralization activity of select purified mAbs. In brief, each antibody was serially diluted (5-fold dilutions) starting at 20 μg/mL. Triplicates of each mAb dilution were incubated with SARS-CoV-2 at a MOI of 0.1 in EMEM with 7.5% inactivated fetal calf serum for 1 hr at 37ºC. Post incubation, the virus-antibody mixture was transferred onto a monolayer of Vero-E6 cells grown overnight. The cells were incubated with the mixture for 70 hrs. CPE were visually scored for each well in a blinded fashion by two independent observers. The results were then converted into percentage neutralization at a given mAb concentration, and the averages ± SEM were plotted using a five-parameter dose-response curve in GraphPad Prism 8.0.

Epitope Mapping by ELISA

50 ng/well of S trimer, 50 ng/well of RBD, and 100 ng/well of NTD were coated on ELISA plates at 4°C overnight. The ELISA plates were then blocked with 300 μL of blocking buffer (1% BSA

514 and 10% bovine calf serum (BCS) (Sigma) in PBS at 37°C for 2 hrs. Afterwards, supernatants
515 from the antibody transfection or purified antibodies were serially diluted using dilution buffer
516 (1% BSA and 20% BCS in PBS), incubated at 37°C for 1 hr. Next, 100 µL of 10,000-fold diluted
517 Peroxidase AffiniPure goat anti-human IgG (H+L) antibody (Jackson ImmunoResearch) were
518 added into each well and incubated for 1 hr at 37°C. The plates were washed between each step
519 with PBST (0.5% Tween-20 in PBS). Finally, the TMB substrate (Sigma) was added and
520 incubated before the reaction was stopped using 1M sulfuric acid. Absorbance was measured at
521 450 nm.
522
523 For the competition ELISA, purified mAbs were biotin-labeled using One-Step Antibody
524 Biotinylation Kit (Miltenyi Biotec) following manufacturer recommendations and purified using
525 40K MWCO Desalting Column (ThermoFisher Scientific). 50 µL of serially diluted competitor
526 antibodies were added into S trimer-precoated ELISA plates, followed by 50 µL of biotinylated
527 antibodies at a concentration that achieves an OD_{450} reading of 1.5 in the absence of competitor
528 antibodies. Plates were incubated at 37°C for 1 hr, and 100 µL of 500-fold diluted Avidin-HRP
529 (ThermoFisher Scientific) were added into each well and incubated for another 1 hr at 37°C. The
530 plates were washed by PBST between each of the previous steps. The plates were developed
531 afterwards with TMB and absorbance was read at 450 nm after the reaction was stopped.
532
533 For the ACE2 competition ELISA, 100 ng of ACE2 protein (Abcam) was immobilized on the
534 plates at 4°C overnight. The unbound ACE2 was washed away by PBST and then the plates were
535 blocked. After washing, 100 ng of S trimer in 50 µL of dilution buffer was added into each well,
536 followed by adding another 50 µL of serially diluted competitor antibodies and then incubating

the plates at 37°C for 1 hr. The ELISA plates were washed 4 times by PBST and then 100 µL of 2000-fold diluted anti-strep-HRP (Millipore Sigma) were added into each well for another 1 hr at 37°C. The plates were then washed, developed with TMB, and absorbance was read at 450 nm after the reaction was stopped.

For all the competition ELISA experiments, the relative binding of biotinylated antibodies or ACE2 to the S trimer in the presence of competitors was normalized by comparing to competitor-free controls. Relative binding curve and the area under curve (AUC) were generated by fitting the non-linear five-parameter dose-response curve in GraphPad Prism 8.0.

Cell-Surface Competition Binding Assay

Expi293 cells were co-transfected with vectors encoding pRRL-cPPT-PGK-GFP (Addgene) and pCMV3-SARS-CoV-2 (2019-nCoV) Spike (Sino Biological) at a ratio of 1:1. Two days after transfection, cells were incubated with a mixture of biotinylated mAb 2-43 (0.25 µg/mL) and serially diluted competitor antibodies at 4°C for 1 hr. Then 100 µL of diluted APC-streptavidin (Biolegend) were added to the cells and incubated at 4°C for 45 mins. Cells were washed 3 times with FACS buffer before each step. Finally, cells were resuspended and 2-43 binding to cell-surface S trimer was quantified on LSRII flow cytometer (BD Biosciences). The mean fluorescence intensity of APC in GFP-positive cells was analyzed using FlowJo and the relative binding of 2-43 to S trimer in the presence of competitors was calculated as the percentage of the mean fluorescence intensity compared to that of the competitor-free controls.

Cryo-EM Data Collection and Processing

SARS-CoV-2 S trimer at a final concentration of 2 mg/ml was incubated with 6-fold molar excess per spike monomer of the antibody Fab fragments for 30 mins in 10 mM Tris-HCl, 150 mM NaCl, and 0.005% n-Dodecyl-β-D-maltoside (DDM). 2 µL of sample were incubated on C-flat 1.2/1.3 carbon grids for 30 secs and vitrified using a Leica EM GP Plunge Freezer. Data were collected on a Titan Krios electron microscope operating at 300 kV equipped with a Gatan K3 direct detector and energy filter using the Leginon software package[34]. A total electron fluence of 51.3 e/Å^2 was fractionated over 40 frames, with a total exposure time of 2 secs. A magnification of 81,000x resulted in a pixel size of 1.058 Å, and a defocus range of -0.4 to -3.5 µm was used. All processing was done using cryoSPARC v2.14.2[35]. Raw movies were aligned and dose-weighted using patch motion correction, and the CTF was estimated using patch CTF estimation. A small subset of approximately 200 micrographs were picked using blob picker, followed by 2D classification and manual curation of particle picks, and used to train a Topaz neural network[36]. This network was then used to pick particles from the remaining micrographs, which were extracted with a box size of 384 pixels.

For the Fab 2-4 dataset, 2D classification followed by *ab initio* modelling and 3D heterogeneous refinement revealed 83,927 particles with three 2-4 Fabs bound, one to each RBD. A reconstruction of these particles using Non-Uniform Refinement with imposed C3 symmetry resulted in a 3.6 Å map, as determined by the gold standard FSC. Given the relatively low resolution of the RBD-Fab interface, masked local refinement was used to obtain a 3.5 Å map with significantly improved density. A masked local refinement of the remainder of the S timer resulted in a 3.5 Å reconstruction. These two local refinements were aligned and combined using the vop maximum function in UCSF Chimera[37]. This was repeated for the half maps, which were used,

583 along with the refinement mask from the global Non-Uniform refinement, to calculate the
584 3DFSC[38] and obtain an estimated resolution of 3.2 Å. All maps have been submitted to the EMDB
585 with the ID EMD-22156.
586
587 For the Fab 4-8 dataset, image preprocessing and particle picking was performed as above. 2D
588 classification, *ab initio* modelling, and 3D heterogeneous classification revealed 47,555 particles
589 with 3 Fabs bound, one to each NTD and with all 3 RBDs in the down conformation. While this
590 particle stack was refined to 3.9 Å using Non-Uniform refinement with imposed C3 symmetry,
591 significant molecular motion prevented the visualization of the Fab epitope at high resolution
592 (EMD-22159). In addition, 105,278 particles were shown to have 3 Fabs bound, but with 1 RBD
593 in the up conformation. These particles were refined to 4.0 Å using Non-Uniform refinement with
594 C1 symmetry (EMD-22158), and suffered from the same conformational flexibility as the all-
595 RBD-down particles. This flexibility was visualized using 3D variability analysis in cryoSPARC.
596
597 For the Fab 2-43 dataset, which was collected at an electron fluence of 53.43 e/Å^2, image
598 preprocessing and particle picking was performed as above, save that motion correction was
599 performed using MotionCor2[39]. 2D classification, *ab initio* modelling, and 3D heterogeneous
600 classification revealed 18,884 particles with 3 Fabs bound, which was refined to 7.8 Å resolution
601 (EMD-22157).
602
603 **Cryo-EM Model Fitting**
604 An initial homology model of the 2-4 Fab was built using Schrodinger Release 2020-2:
605 BioLuminate[40]. The RBD was initially modeled using the coordinates from PDB ID 6W41. The

606 remainder of the S timer was modeled using the coordinates from PDB ID 6VSB. These models
607 were docked into the consensus map using Chimera. The model was then fitted interactively using
608 ISOLDE 1.0b5[41] and COOT 0.8.9.2[42], and using real space refinement in Phenix 1.18[43]. In cases
609 where side chains were not visible in the experimental data, they were truncated to alanine.
610 Validation was performed using Molprobity[44] and EMRinger[45]. The model was submitted to the
611 PDB with the ID 6XEY. Figures were prepared using ChimeraX[46].

Methods references

26 Schramm, C. A. *et al.* SONAR: A High-Throughput Pipeline for Inferring Antibody Ontogenies from Longitudinal Sequencing of B Cell Transcripts. *Frontiers in immunology* **7**, 372, doi:10.3389/fimmu.2016.00372 (2016).

27 Altschul, S. F. *et al.* Gapped BLAST and PSI-BLAST: a new generation of protein database search programs. *Nucleic Acids Res* **25**, 3389-3402 (1997).

28 Lefranc, M. P. *et al.* IMGT, the international ImMunoGeneTics information system. *Nucleic Acids Res* **37**, D1006-1012, doi:10.1093/nar/gkn838 (2009).

29 Sievers, F. & Higgins, D. G. Clustal Omega, Accurate Alignment of Very Large Numbers of Sequences. *Multiple Sequence Alignment Methods* **1079**, 105-116, doi:10.1007/978-1-62703-646-7_6 (2014).

30 Edgar, R. C. Search and clustering orders of magnitude faster than BLAST. *Bioinformatics* **26**, 2460-2461, doi:10.1093/bioinformatics/btq461 (2010).

31 Sheng, Z. *et al.* Gene-Specific Substitution Profiles Describe the Types and Frequencies of Amino Acid Changes during Antibody Somatic Hypermutation. *Frontiers in immunology* **8**, 537 (2017).

32 Nie, J. *et al.* Establishment and validation of a pseudovirus neutralization assay for SARS-CoV-2. *Emerg Microbes Infect* **9**, 680-686, doi:10.1080/22221751.2020.1743767 (2020).

33 Whitt, M. A. Generation of VSV pseudotypes using recombinant DeltaG-VSV for studies on virus entry, identification of entry inhibitors, and immune responses to vaccines. *J Virol Methods* **169**, 365-374, doi:10.1016/j.jviromet.2010.08.006 (2010).

34 Suloway, C. *et al.* Automated molecular microscopy: the new Leginon system. *J Struct Biol* **151**, 41-60, doi:10.1016/j.jsb.2005.03.010 (2005).

35 Punjani, A., Rubinstein, J. L., Fleet, D. J. & Brubaker, M. A. cryoSPARC: algorithms for rapid unsupervised cryo-EM structure determination. *Nat Methods* **14**, 290-296, doi:10.1038/nmeth.4169 (2017).

36 Bepler, T. *et al.* Positive-unlabeled convolutional neural networks for particle picking in cryo-electron micrographs. *Nature Methods* **16**, 1153-1160, doi:10.1038/s41592-019-0575-8 (2019).

37 Pettersen, E. F. *et al.* UCSF Chimera--a visualization system for exploratory research and analysis. *J Comput Chem* **25**, 1605-1612, doi:10.1002/jcc.20084 (2004).

38 Tan, Y. Z. *et al.* Addressing preferred specimen orientation in single-particle cryo-EM through tilting. *Nat Methods* **14**, 793-796, doi:10.1038/nmeth.4347 (2017).

39 Zheng, S. Q. *et al.* MotionCor2: anisotropic correction of beam-induced motion for improved cryo-electron microscopy. *Nat Methods* **14**, 331-332, doi:10.1038/nmeth.4193 (2017).

40 Zhu, K. *et al.* Antibody structure determination using a combination of homology modeling, energy-based refinement, and loop prediction. *Proteins* **82**, 1646-1655, doi:10.1002/prot.24551 (2014).

41 Croll, T. I. ISOLDE: a physically realistic environment for model building into low-resolution electron-density maps. *Acta Crystallogr D Struct Biol* **74**, 519-530, doi:10.1107/S2059798318002425 (2018).

42 Emsley, P. & Cowtan, K. Coot: model-building tools for molecular graphics. *Acta Crystallogr D Biol Crystallogr* **60**, 2126-2132, doi:10.1107/S0907444904019158 (2004).

43 Adams, P. D. *et al.* Recent developments in the PHENIX software for automated crystallographic structure determination. *J Synchrotron Radiat* **11**, 53-55, doi:10.1107/s0909049503024130 (2004).

44 Davis, I. W., Murray, L. W., Richardson, J. S. & Richardson, D. C. MOLPROBITY: structure validation and all-atom contact analysis for nucleic acids and their complexes. *Nucleic Acids Res* **32**, W615-619, doi:10.1093/nar/gkh398 (2004).

45 Barad, B. A. *et al.* EMRinger: side chain-directed model and map validation for 3D cryo-electron microscopy. *Nat Methods* **12**, 943-946, doi:10.1038/nmeth.3541 (2015).

46 Goddard, T. D. *et al.* UCSF ChimeraX: Meeting modern challenges in visualization and analysis. *Protein Sci* **27**, 14-25, doi:10.1002/pro.3235 (2018).

Acknowledgements

We thank Nianshuang Wang and Jason McLellan for providing reagents for generating the SARS-CoV-2 S trimer and RBD-SD1 with mFc tag. We thank Wendy Chen for assistance with generating the Venn diagrams, and Brandon Dekosky and Xueling Wu for helpful input. This study was supported by funding to D.D.H. from the Jack Ma Foundation, the JPB Foundation, Samuel Yin, Roger Wu, and Carol Ludwig. Cryo-EM data collection was performed at the National Center for CryoEM Access and Training (NCCAT) and the Simons Electron Microscopy Center located at the New York Structural Biology Center, supported by the NIH Common Fund Transformative High Resolution Cryo-Electron Microscopy program (U24 GM129539) and by grants from the Simons Foundation (SF349247) and NY State Assembly. Data analysis was performed at the National Resource for Automated Molecular Microscopy (NRAMM), supported by the NIH National Institute of General Medical Sciences (GM103310).

Author Contributions

D.D.H conceived of the project. L.L., P.W., M.S.N, J.Y., Y.H. performed many of the experiments. M.T.Y. was responsible for recruiting patients, obtaining clinical specimens, and summarizing clinical data. L.L., V.S., A.F. and X.V.G. performed and analyzed the B-cell sorting, 10X Genomics, sequencing and analysis of the clones. Z.S. performed bioinformatic analyses on 10X next-generation sequencing data and antibody repertoire. J.Y. cloned, expressed, and purified the mAbs. L.L. and Q.W. performed the epitope mapping and binding experiments. P.W. conducted the pseudovirus neutralization assays and M.S.N. and Y.X. performed infectious SARS-CoV-2 neutralization assays. M.A.R., G.C., J.B, J.G., and L.S. carried out the cryo-EM studies. Y.L. helped with project management. T.Z. and P.D.K. provided key reagents for the study, and

691 P.D.K. contributed to the analysis and discussion of the data. L.L., P.W., M.S.N., J.Y., Y.H., Z.S.,
692 M.A.R., Q.W, L.S., and D.D.H analyzed the results, and D.D.H. wrote the manuscript, with
693 contributions from each author. J.G.S. provided valuable suggestions.
694
695 **Competing Interest Declaration**
696 A provisional patent application has been filed for the monoclonal antibodies described in the
697 manuscript.

Extended Data

Extended Data Table 1 Patient information

Patient	Age	Sex & Race	Days from symptom onset to:	Biomarker	Complications	Outcome
1	57	Female, Hispanic	Admission: 7 MV: 12 Ab isolation: 18	hsCRP = 208 mg/L ESR = 58 mm/hr IL-6 = 23 pg/mL Ferritin = 766 ng/mL D-dimer = 3.4 μg/mL FEU	ARDS	Discharged on day 30
2	71	Female, Hispanic	Admission: 20 MV: 20 Ab isolation: 29	hsCRP = 33 mg/L ESR > 130 mm/hr IL-6 = 13 pg/mL Ferritin = 425 ng/mL D-dimer = 5.7 μg/mL FEU	ARDS Ventilator associated pneumonia	Discharged on day 45
3	61	Male, White	Admission: 10 MV: 10 Ab isolation: 21	hsCRP = 51 mg/L ESR = 57 mm/hr IL-6 > 315 pg/mL Ferritin = 3,238 ng/mL D-dimer = 7.4 μg/mL FEU	ARDS Acute kidney injury (hemodialysis) Sepsis	Death on day 28
4	51	Male, Black	Admission: 7 MV: 10 Ab isolation: 25	hsCRP = 88 mg/L ESR = 110 mm/hr IL-6 = 77 pg/mL Ferritin = 510 ng/mL D-dimer = 13.4 μg/mL FEU	ARDS Acute kidney injury (no hemodialysis) Ventilator associated pneumonia	Discharged on day 51
5	50	Male, White	Admission: 5 MV: 7 Ab isolation: 32	hsCRP = 2 mg/L ESR = 63 mm/hr	ARDS Neuropathy	Discharged on day 27

Abbreviation: ARDS, acute respiratory distress syndrome; MV, mechanical ventilation; hsCRP, high sensitivity C-reactive protein, ULN>10 mg/L; ESR, erythrocyte sedimentation rate, ULN=20 mm/hr; Interleukin 6, ULN= 5 pg/mL; Ferritin, ULN=150 ng/mL; D-dimer quantitative ULN= 0.8μg/mL FEU.

705 **Extended Data Table 2 Summary of mAb screening.**

	Abs	Binding Abs			Neutralizing Abs	
		S trimer	RBD	Non-RBD	Pseudovirus	Live virus
Total	252	121	38	83	61	41
Patient 1	100	45	19	26	19	11
Patient 2	54	29	12	17	18	18
Patient 3	6	2	0	2	3	0
Patient 4	44	32	7	25	14	6
Patient 5	48	13	0	13	7	6

706 **Extended Data Table 3 Cryo-EM data collection, refinement, and validation statistics**.

	SARS-CoV-2 spike with Fab 2-4 (EMDB-22156) (PDB 6XEY)	SARS-CoV-2 spike RBD up with Fab 4-8 EMDB-22158	SARS-CoV-2 spike RBD down with Fab 4-8 EMDB-22159	SARS-CoV-2 spike with Fab 2-43 EMDB-22157
Data collection and processing				
Magnification	81,000	81,000	81,000	81,000
Voltage (kV)	300	300	300	300
Electron exposure (e–/Å^2)	51.30	51.30	51.30	53.43
Defocus range (μm)	-0.4 to -3.5	-0.4 to -3.5	-0.4 to -3.5	-0.4 to -3.5
Pixel size (Å)	1.058	1.058	1.058	1.058
Symmetry imposed	C3	C1	C3	C1
Initial particle images (no.)	556,983	256,848	256,848	709,052
Final particle images (no.)	83,927	105,278	47,555	18,885
Map resolution (Å)	3.25	4.0	3.9	7.8
FSC threshold	0.143	0.143	0.143	0.143
Map resolution range (Å)	406.3-3.25	406.3-4.0	406.3-3.9	406.3-7.8
Refinement				
Initial model used (PDB code)	6VSB			
Model resolution (Å)	3.7			
FSC threshold	0.5			
Model resolution range (Å)	406.3-3.25			
Map sharpening *B* factor (Å^2)	-97.5			
Model composition				
Non-hydrogen atoms	28,672			
Protein residues	3785			
Ligands	63			
B factors (Å^2)				
Protein	60.89			
Ligand	50.00			
R.m.s. deviations				
Bond lengths (Å)	0.012			
Bond angles (°)	1.879			
Validation				
MolProbity score	1.05			
Clashscore	0.16			
Poor rotamers (%)	0.25			
Ramachandran plot				
Favored (%)	92.09			
Allowed (%)	7.77			
Disallowed (%)	0.13			

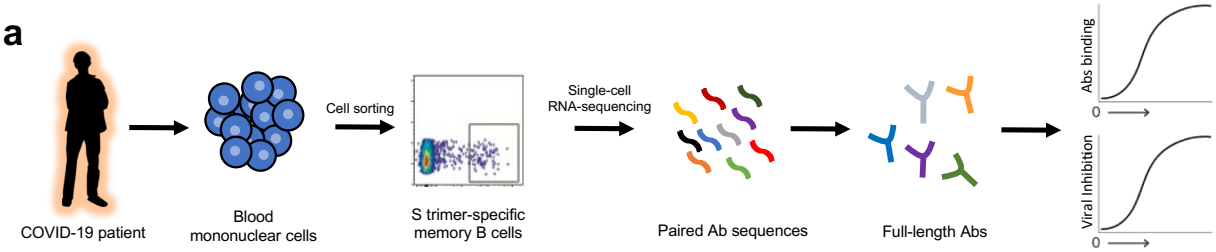

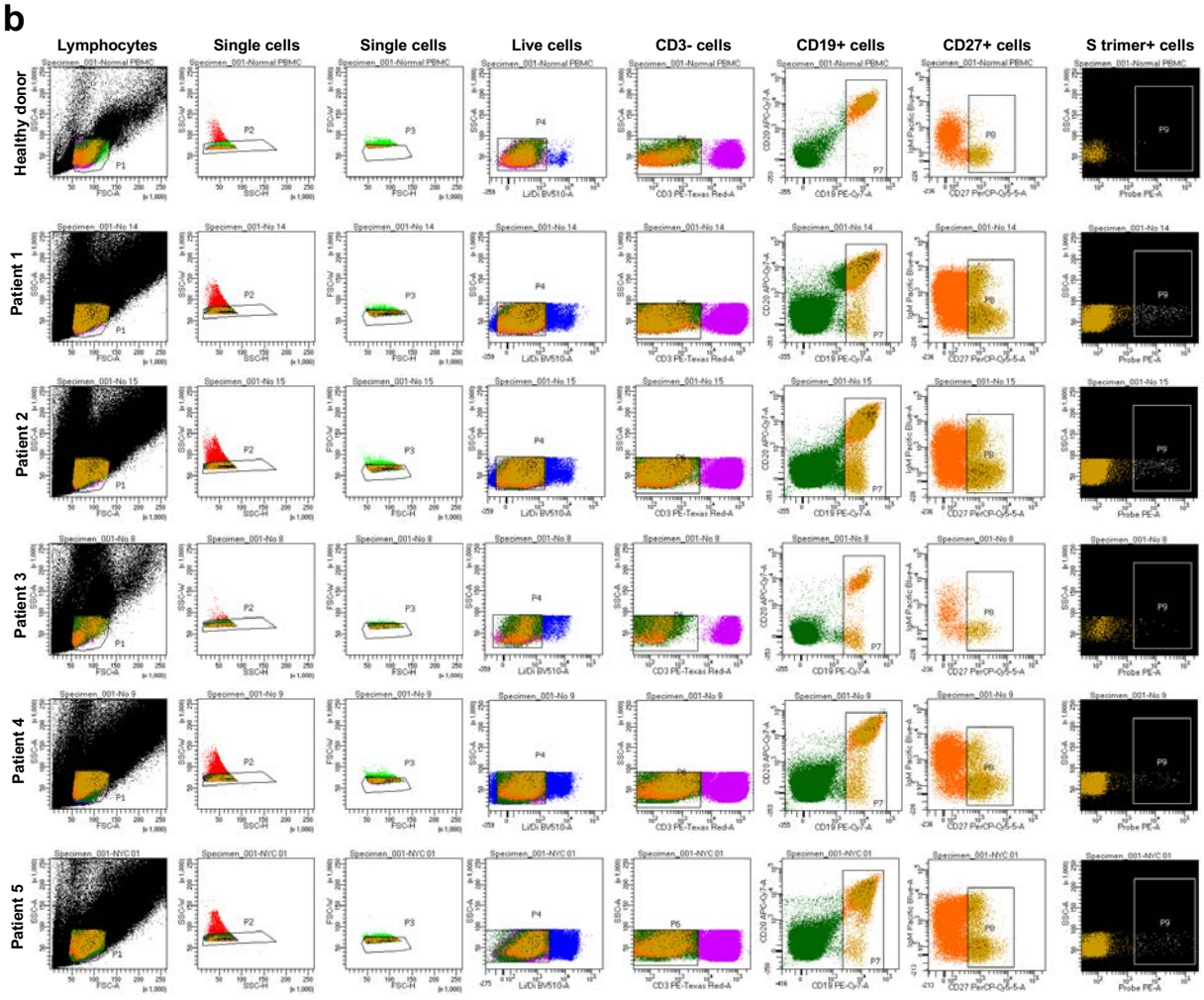

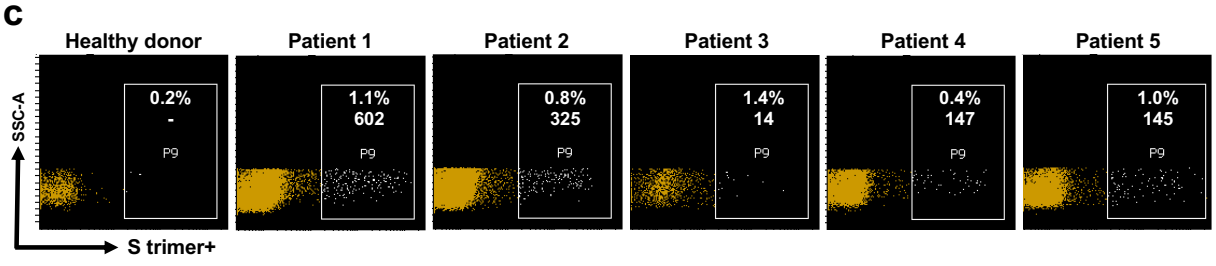

Extended Data Fig. 1 SARS-CoV-2 S trimer-specific antibody isolation strategy. a, Schema for isolating of S trimer-specific mAbs from memory B cells in the blood of infected patients. **b**, Sorting results on the isolation of S trimer-specific memory B cells using flow cytometry. **c**, Magnified representation of the panel of S trimer-positive memory B cells for each patient. Inset numbers indicate the absolute number and the percentage of S trimer-specific memory B cells isolated from each case.

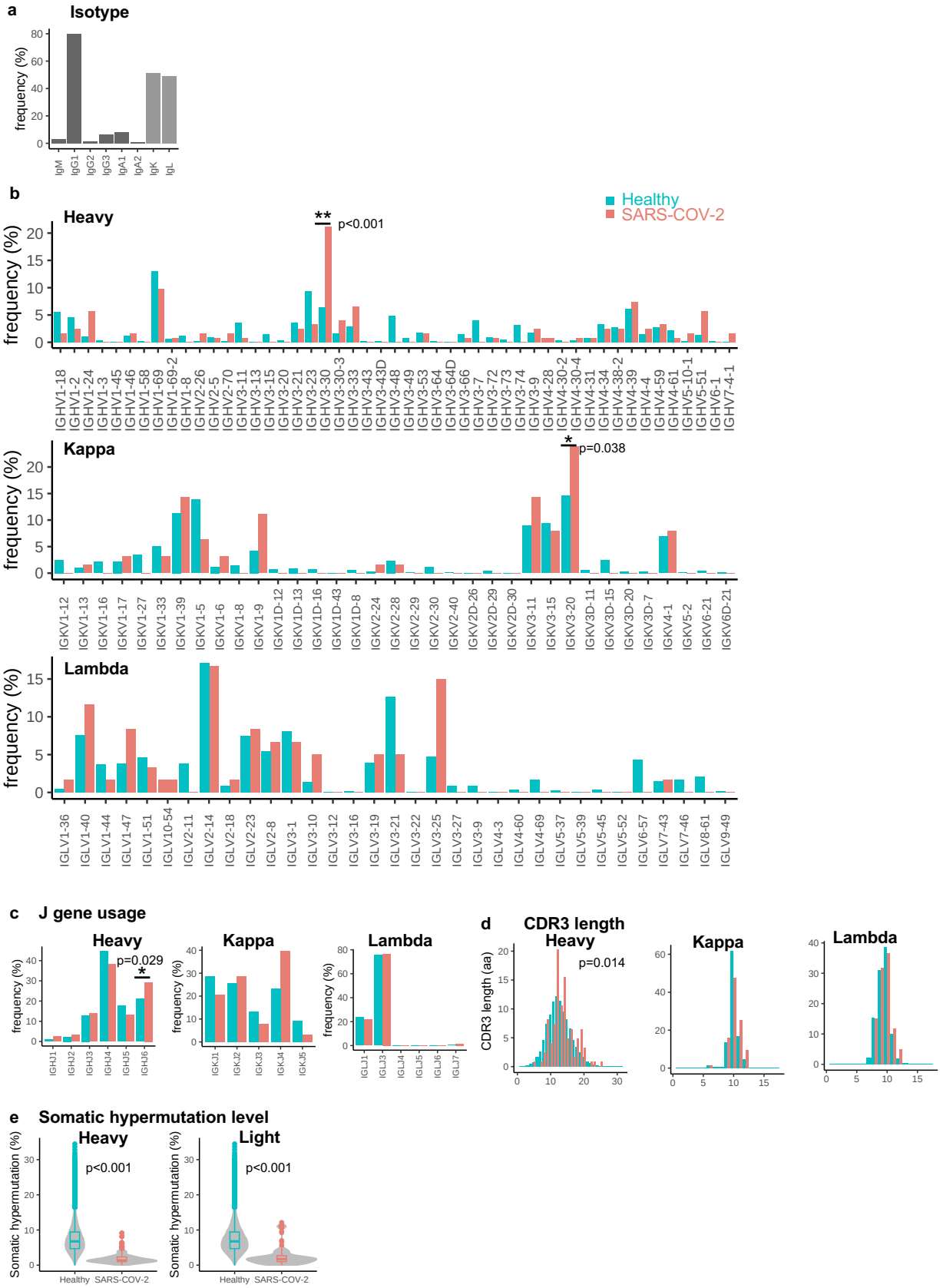

Extended Data Fig. 2 Genetic features of SARS-CoV-2-specific antibody repertoire. a, Most of the 121 trimer S-specific antibodies are of IgG isotype. The kappa and lambda light chains are comparably used. **b**, Compared to IgG repertoires of healthy human donors, IGHV3-30 and IGKV3-20 genes are over-represented in heavy and light chain repertoires, respectively (ß2-test, $p<0.05$). **c**, The usage of IGHJ6 gene was significantly higher in antigen-specific antibodies (ß2-test, $p<0.05$). **d**, The CDRH3 length of antigen-specific antibodies is significantly longer than in healthy donors (Kolmogorov–Smirnov test, $p=0.014$). **e**, For both heavy and light chains, the V region nucleotide somatic hypermutation levels are significantly lower than in antibodies of healthy donors (Kolmogorov–Smirnov test, $p<0.001$).

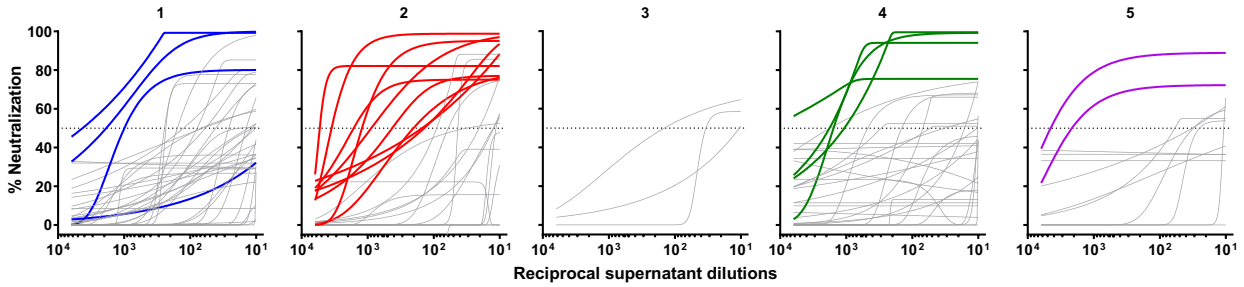

Extended Data Fig. 3 The best-fit pseudovirus neutralization curves for 130 samples that were positive in at least one of the screens shown in Fig. 1b. The 18 transfection supernatants that showed evidently better potency are highlighted in colors, while others with non-neutralizing or weakly neutralizing activities are shown in grey. One additional supernatant (Patient 1) that was initially missed in the pseudovirus screen but later found to be a potent neutralizing mAb (1-87) is also highlighted.

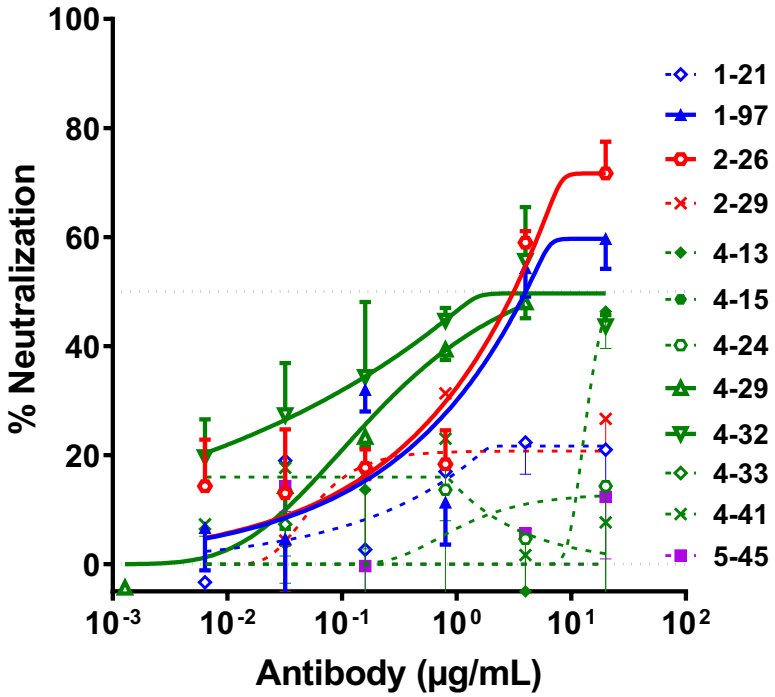

731 **Extended Data Fig. 4 The pseudovirus neutralization profiles for 12 purified mAbs that**
732 **strongly bound the S trimer but with weak or no virus-neutralizing activities.** The four mAbs
733 with weak neutralizing activities against SARS-CoV-2 pseudovirus are shown in sold lines, and
734 the remaining 8 non-neutralizing mAbs are shown in dashed lines.

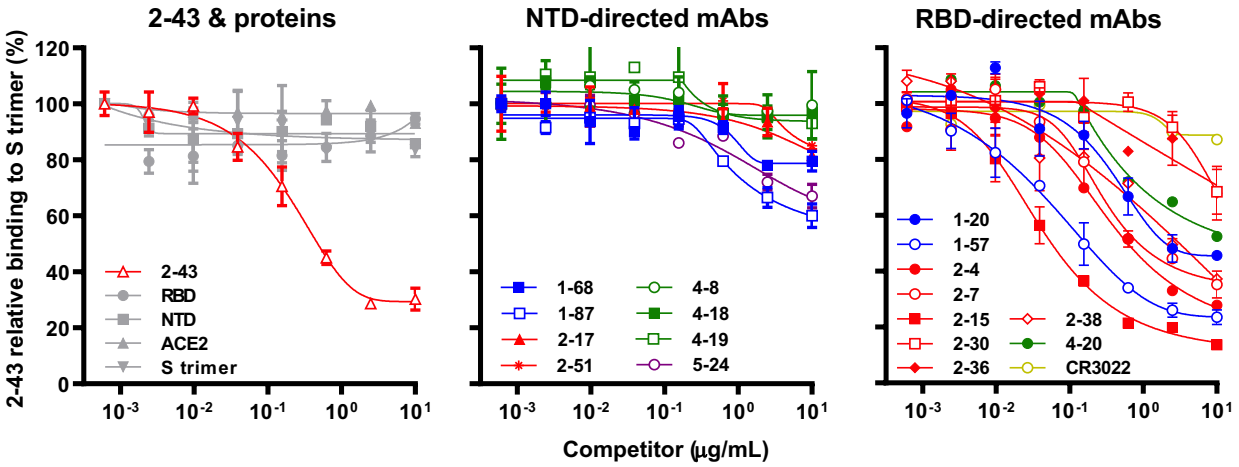

735

736 **Extended Data Fig. 5 Monoclonal Ab 2-43 bound to S trimer expressed on Expi293 cell**

737 **surface can be competed out by mAbs directed to RBD but only minimally by mAbs to the**

738 **NTD region.**

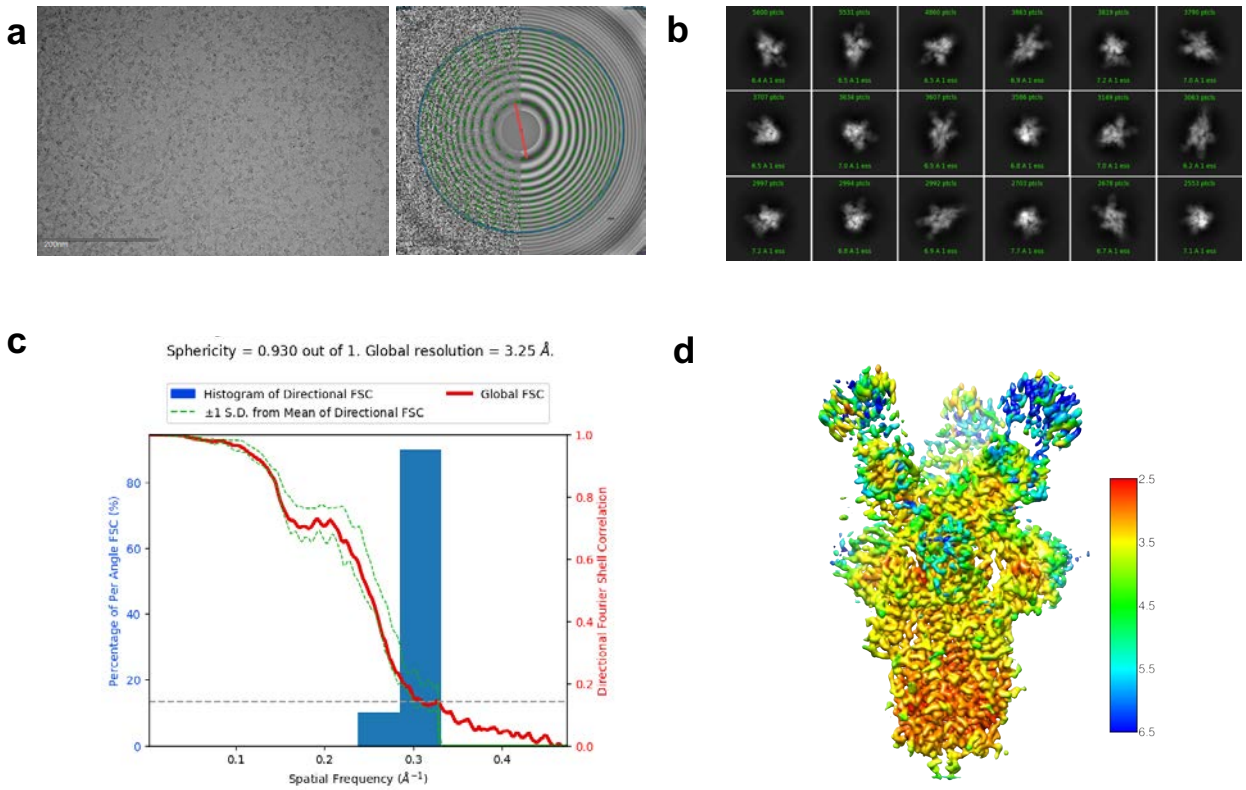

739

740 **Extended Data Fig. 6 Cryo-EM data processing for antibody 2-4 in complex with the S**
741 **trimer. a,** Representative micrograph and CTF of the micrograph. **b**, Representative 2D class
742 averages. **c,** Resolution of the consensus map with C3 symmetry as calculated by 3DFSC. **d,** The
743 local resolution of the full map as calculated by cryoSPARC at an FSC cutoff of 0.5. **e,**
744 Representative density of the Fab 2-4 and RBD interface, showing CRR H3, L3, and L3 (left),
745 along with CDR H2 and the N-linked glycosylation at ASN58 (right).

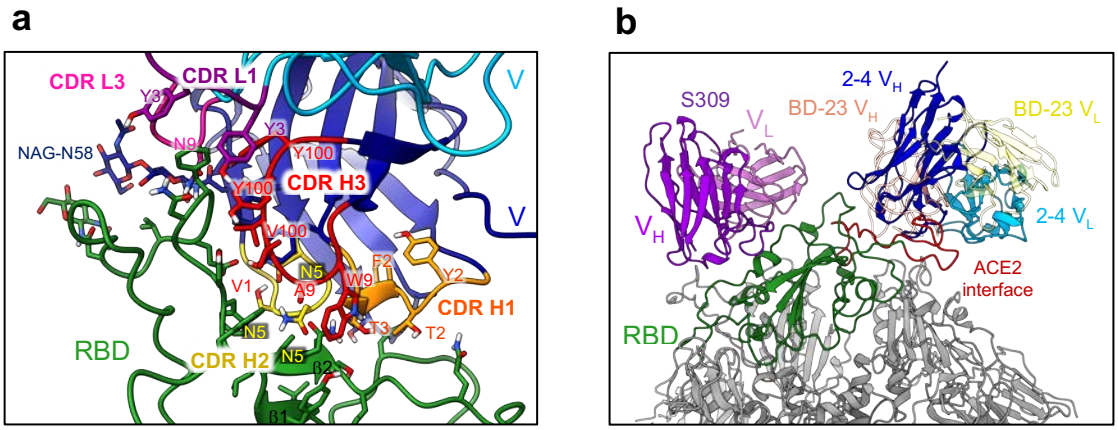

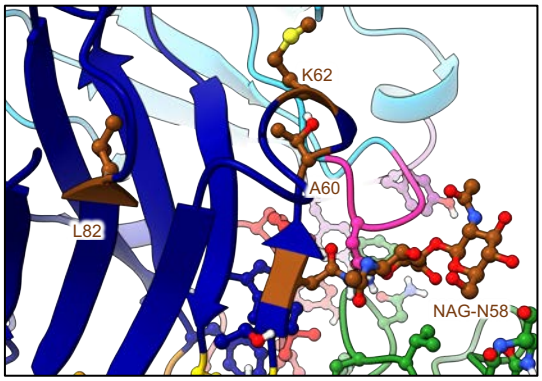

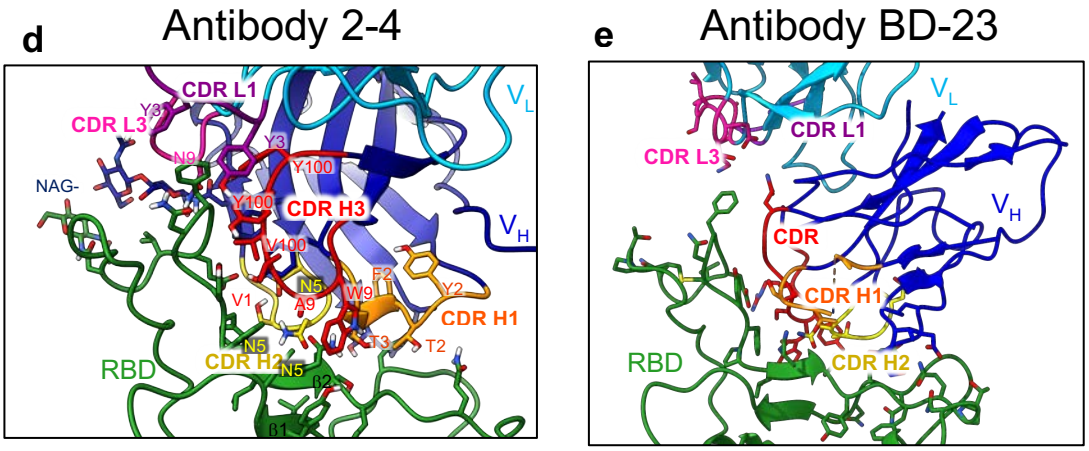

747 **Extended Data Fig. 7 a,** Fab 2-4 binding interface with RBD. **b**, Positions of antibodies 2-4,
748 S309[8], and BD-23[9] on the trimeric CoV-2 spike. **c,** Somatic hypermutations found only in the
749 antibody 2-4 heavy chain, shown in brown. The mutation A60T creates an NxT sequence leading
750 to N58 glycosylation. **d,** Antibody 2-4 in complex with S trimer. CDR loops are indicated in colors,
751 and side chains are shown for interacting residues. **e,** Antibody BD-23[9] in complex with S trimer.

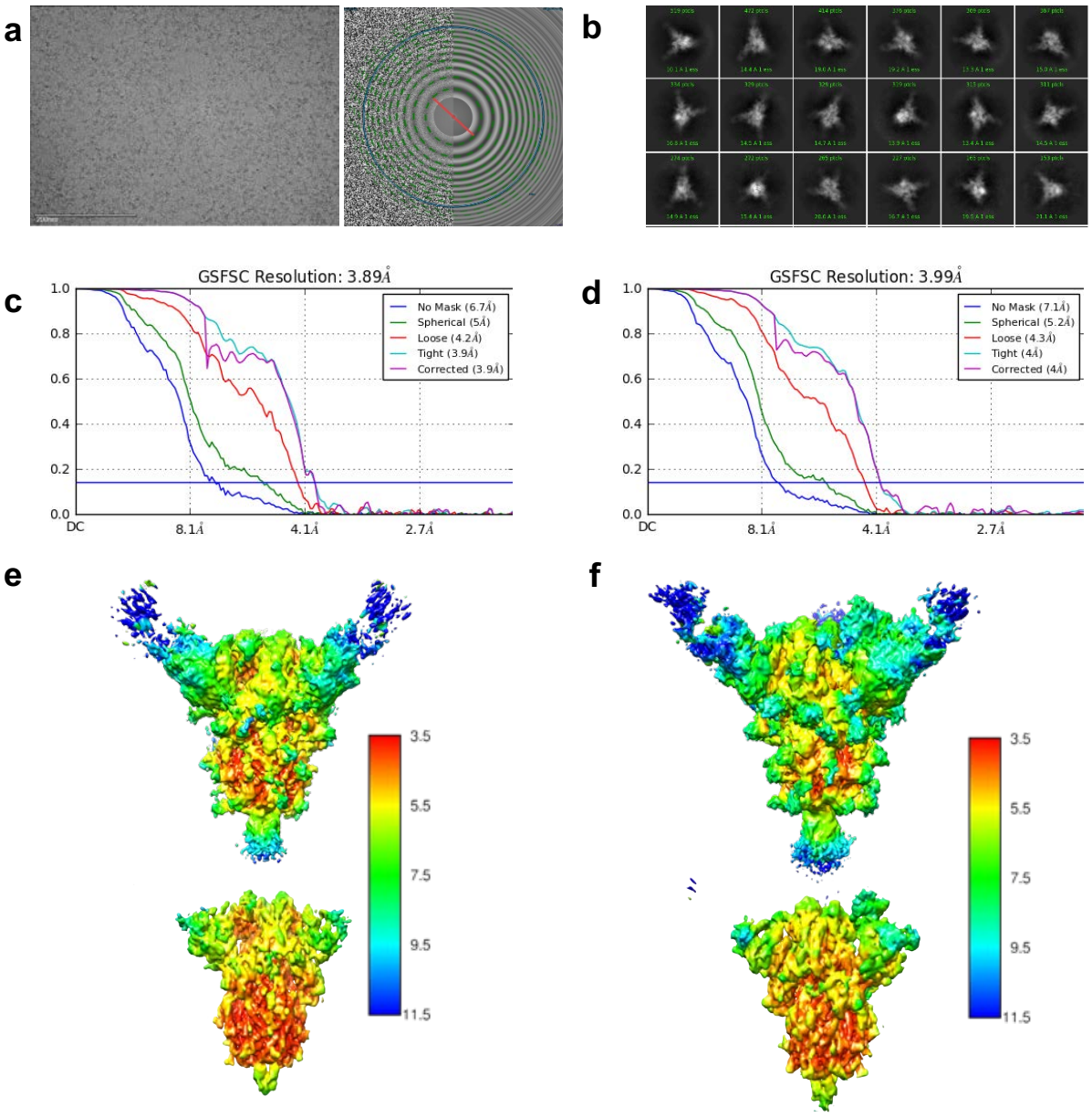

752 **Extended Data Fig. 8 Cryo-EM data processing for antibody 4-8 in complex with the S**
753 **trimer. a,** Representative micrograph and CTF of the micrograph. **b**, Representative 2D class
754 averages. **c,** Resolution of the spike in the RBD down conformation in complex with Fab 4-8 **d,**
755 Resolution of the spike in the RBD up conformation in complex with Fab 4-8. **e,** Local resolution
756 of the spike in the RBD down conformation in complex with Fab 4-8 at an FSC cutoff of 0.5. Two

757 thresholds are shown. **f,** Local resolution of the spike in the RBD up conformation in complex with

758 Fab 4-8 at an FSC cutoff of 0.5. Two thresholds are shown.

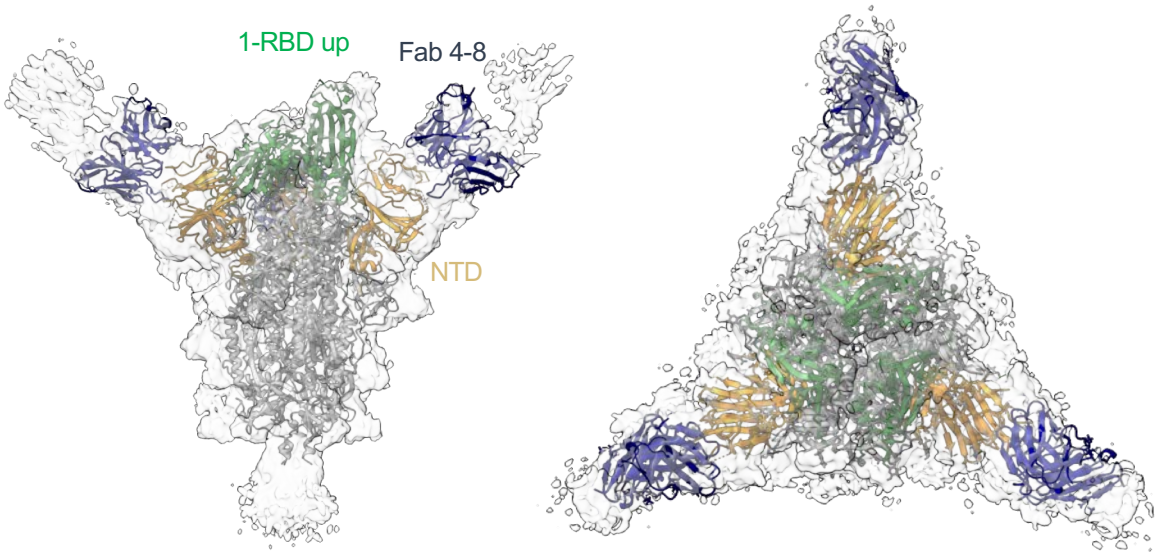

759 **Extended Data Fig. 9 3D reconstructions of NTD-targeting neutralizing antibody 4-8 in complex**

760 **with the SARS-CoV-2 spike trimer with the 1-RBD-up conformation.**

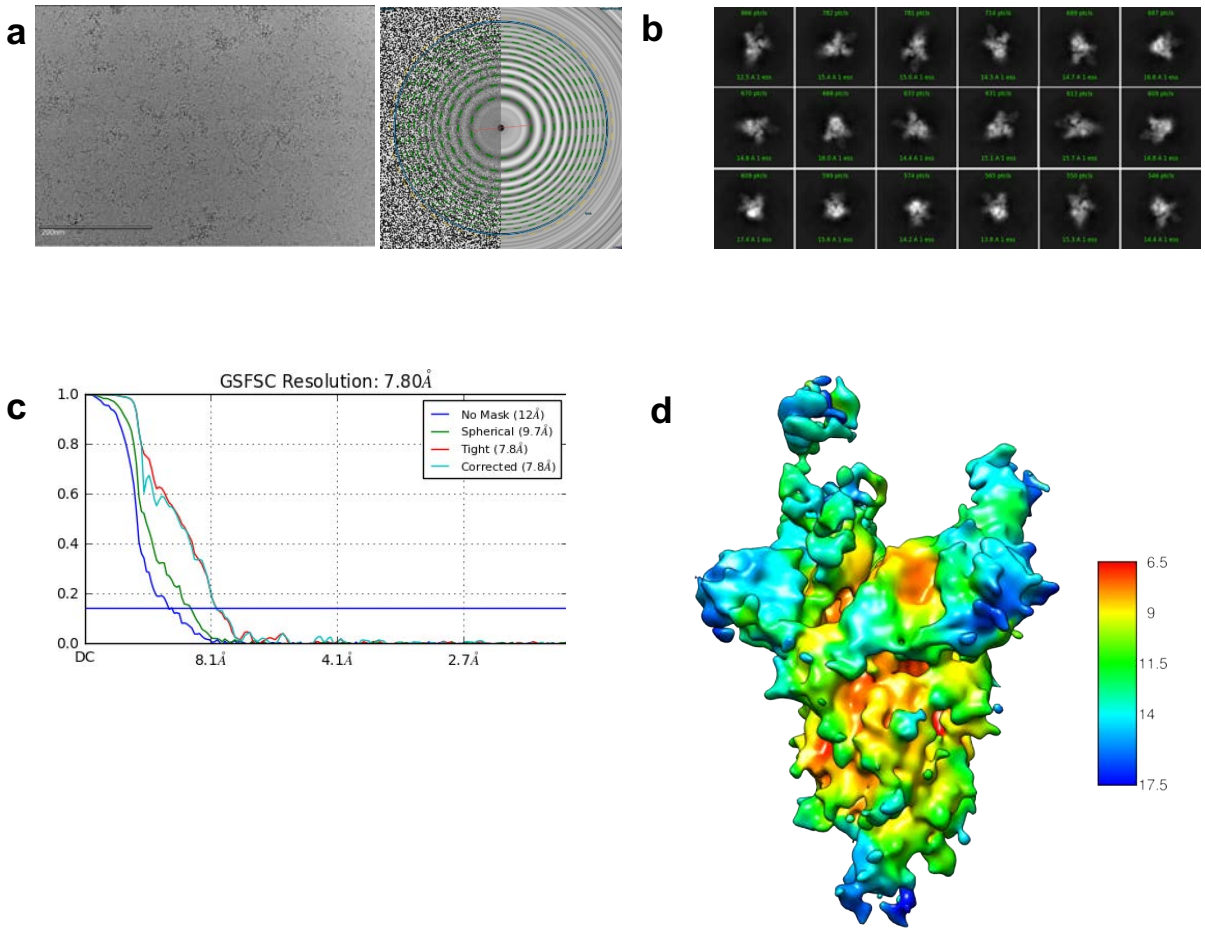

761 **Extended Data Fig. 10 Cryo-EM data processing for antibody 2-43 in complex with the S**

762 **trimer. a,** Representative micrograph and CTF of the micrograph. **b**, Representative 2D class

763 averages. **c,** Resolution of Fab 2-43 in complex with S trimer. **d,** The local resolution of the full

764 map as calculated by cryoSPARC at an FSC cutoff of 0.5.